Spin Injection from a Ferromagnetic Insulator into a Superconductor

M. Matsuo and T. Kato

Spin injection from a ferromagnetic metal into a superconductor (SC) has been investigated for a long time. For conventional s-wave superconductors, spin injection is suppressed by a SC energy gap. Thermally excited quasiparticles in SC, however, can carry injected spins over long distances, as spin excitations in SCs have long lifetimes. Several novel techniques for spin injection have been developed so far. For example, the spin injection can be realized by the spin Seebeck effect under a temperature gradient, or by applying a spin pumping protocol using ferromagnetic resonance (FMR) under microwave irradiation.

Recently, spin injection from a ferromagnetic insulator (FI) into a SC has also been performed [1]. Although this study opens up possible applications for novel superconducting spintronic devices using FI, spin injection from a FI has been studied theoretically only in Ref. [2] in the context of the damping in the FMR experiments. In the present study [3], we considered a bilayer system composed of a *s*-wave singlet SC and a FI as shown in Fig. 1(a), and calculated the spin current induced by the spin Seebeck effect or spin pumping, using the perturbation theory with respect to the interface exchange interaction.

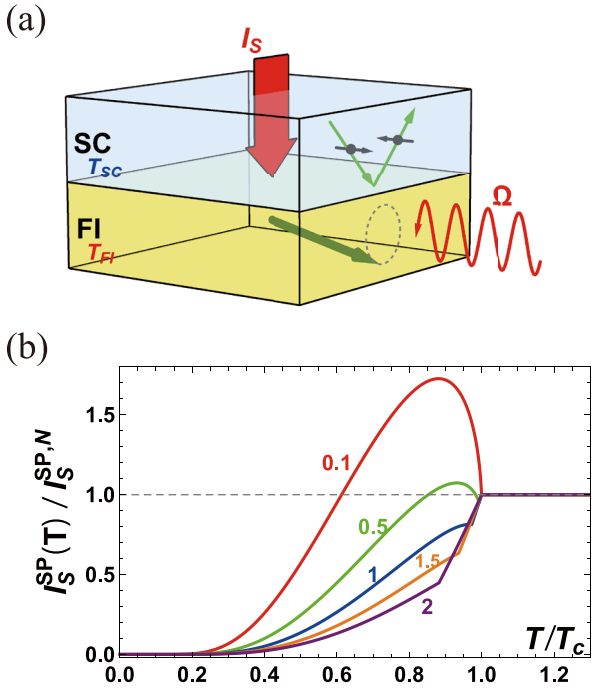

Fig. 1. (a) A schematic of the bilayer system composed of a superconductor (SC) and a ferromagnetic insulator (FI). (b) The temperature dependence of the spin current induced by spin pumping under microwave irradiation. The curves correspond to $\hbar\Omega/k_BT_C$ =0.1, 0.5, 1, 1.5, and 2 from the top to the bottom.

In Fig. 1(b), we show the temperature dependence of the spin current induced by spin pumping. Here the temperature of the bilayer system and the spin current are normalized by the SC transition temperatures T_C and the spin current for a normal metal, respectively. For small excitation frequency Ω, the spin current is enhanced below the SC transition temperature due to a coherent factor in analogy with the NMR measurement. For $\hbar\Omega < 2\Delta(T = 0) \approx 3.54k_BT_C$, the spin current is strongly reduced at low temperatures ($k_BT \ll 2\Delta(T)$, because spin-flip excitations in the SC are suppressed due to the energy gap 2Δ in the one-electron excitation spectrum, where $\Delta(T)$ is the SC energy gap (a function of the temperature T). As Ω increases, the coherence peak becomes insignificant, while there appears a kink at the temperature satisfying $2\Delta(T) = \hbar\Omega$. For $\hbar\Omega > 2\Delta(T = 0)$, the spin current shows a plateau at a low temperature corresponding to its zero temperature value, ultimately recovering the normal state value (dashed line) as Ω increases further. We also calculated the spin current induced by the spin Seebeck effect (not shown here), and discussed the effect of the SC transition.

For a realistic experimental setup, we estimated the noise power of the pure spin current following the theory developed in Ref. [4]. We have shown that the nonequilibrium spin-current noise in spin pumping experiments is much larger than the thermal noise at low temperatures, and that both noises show a coherent peak below the SC transition temperature. Finally, we proposed a possible experimental setup to measure the spin current and its noise obtained here, utilizing the inverse spin Hall effect in SCs.

This study has been performed as a joint study extended from the previous study [4] with Mamoru Matsuo, who was a visiting professor of ISSP in the academic year 2016. This study has also been performed as a collaborated project with the French group (the leader is Thierry Martin at Aix Marseille Univ., CPT, Marseille).

References

[1] M. Umeda *et al.*, App. Phys. Lett. **112**, 232601 (2018).
[2] M. Inoue, M. Ichioka, and H. Adachi, Phys. Rev. B **96**, 024414 (2017).
[3] T. Kato, Y. Ohnuma, M. Matsuo, J. Rech, T. Jonckheere, and T. Martin, Phys. Rev. B **99**, 144411 (2019).
[4] M. Matsuo, Y. Ohnuma, T. Kato, and S. Maekawa, Phys. Rev. Lett. **120**, 037201 (2018).

Authors
T. Kato, Y. Ohnuma[a], M. Matsuo[a], J. Rech[b], T. Jonckheere[b], and T. Martin[b]
[a]Kavli Institute for Theoretical Sciences, University of Chinese Academy of Sciences
[b]Aix Marseille Univ, Université de Toulon, CNRS, CPT

Turning a Graphene into a Topological Insulator with Surface Decoration

J. Haruyama, S. Katsumoto, and T. Nakamura

Graphene once played a key role in the development of topological insulators, which exhibit an electrically inert interior yet form metallic states at their boundary (the edge states). Kane and Mele, in 2005, predicted that coupling between the spin and orbital motion of electrons turns graphene (or some honeycomb lattice) into a 'quantum-spin-Hall (QSH)' insulator that hosts spin-filtered metallic edge states with inherent resilience from scattering. These novel edge states underlie tantalizing technological applications for low-power electronics, spintronic devices, and fault-tolerant quantum computing. Although graphene's intrinsic spin-orbit coupling is far too weak to produce an observable QSH phase in practice, numerous alternative platforms were subsequently discovered, including HgTe and InAs/GaSb quantum wells, WTe_2, bismuthene, and the layered compound $Bi_{14}Rh_3I_9$.

Realization of the QSH effect in graphene devices has remained an outstanding challenge dating back to the inception of the field of topological insulators. Graphene's exceptionally weak spin-orbit coupling—stemming from carbon's low mass—poses the primary obstacle. We experimentally study artificially enhanced spin-orbit coupling in graphene via random decoration with dilute Bi_2Te_3 nanoparticles. Remarkably, multi-terminal resistance measurements suggest the presence of helical edge states characteristic of a QSH phase; those magnetic-field and temperature dependence, X-ray photoelectron spectra, scanning tunneling spectroscopy, and first-principles calculations further support this scenario. These observations highlight a pathway to spintronics and quantum-information applications in graphene-based QSH platforms.

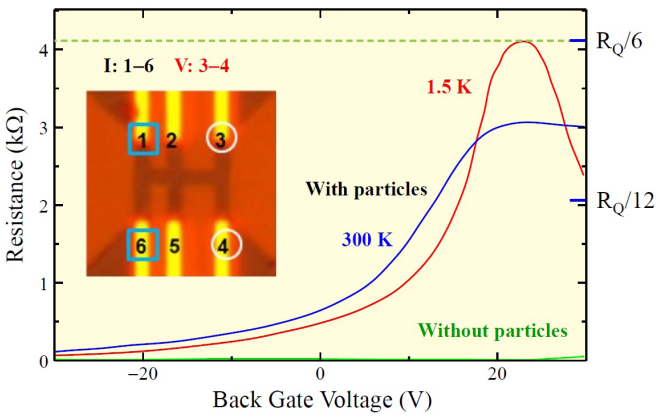

Fig. 1. Inset: AFM image of the sample. The vague dark regions are fabricated graphene with fine particles. The yellow-colored regions are Au electrodes. The blue squares indicate the current electrodes and the white circles the voltage electrodes. At 1.5 K, with varing the back gate voltage, the resistance increases and hits 1/6 of the quanutm resistance, which is just expected for the configuration of the electrodes and perfect conductance connection between them.

References

[1] K. Hatsuda, H. Mine, T. Nakamura, J. Li, R. Wu, S. Katsumoto, and J. Haruyama, Sci. Adv. **4**, eaau6915 (2018).

Authors

J. Haruyama[a], K. Hatsuda[a], S. Katsumoto, and T. Nakamura

[a]Aoyama-Gakuin University

Coexisting Two Types of Spin Splitting Originating from Different Orbital Symmetries

K. Yaji, S. Tanaka, and F. Komori

Spin degeneracy of conducting electrons in materials can be lifted by spin-orbit interaction (SOI). Here, the symmetry of a surface or interface plays an important role in determining the spin splitting and texture of a 2D band. [1] In the framework of the Rashba model for a two-dimensional (2D) electron gas, a free-electron-like band dispersing from the Γ point is shifted oppositely in the wave number direction by SOI, depending on the spin direction that is perpendicular to both the surface normal and momentum of the electron. Another type of the spin-split band in the 2D system is called the Zeeman type, where the spin direction is perpendicular to the 2D plane without spin degeneracy at the symmetry point in the wave-number space. In the case of the spin-split bands of the surface 2D electron system with a three-fold lattice symmetry, either the Zeeman- or Rashba-type spin splitting has been considered to appear around a K point exclusively depending on the crystal symmetry. [1]

We have found a novel spin-dependent band structure of a Sn triangular-lattice atomic layer (TLAL) at the K point. The sample is formed by intercalation into the interface between graphene and the SiC(0001) substrate as a schematic model shown in Fig. 1(a). [2] At the K point of the Sn TLAL with the symmetry of C_3 according to the lattice symmetry *p3m1*, the Zeeman-type spin splitting is reason-

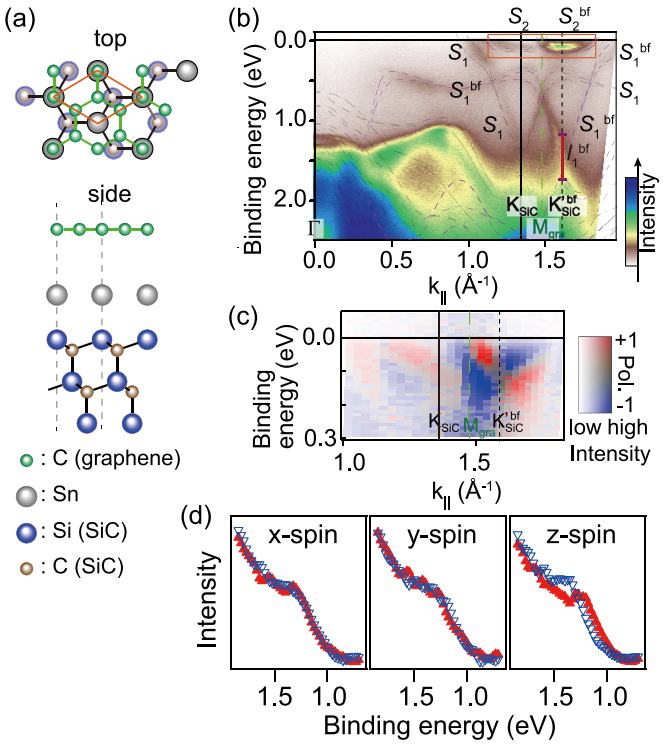

Fig. 1 (a) Atomic structure model of a Sn TLAL intercalated into the graphene/SiC(0001) interface. (b) ARPES intensity image of the Sn TLAL along ΓK_{SiC} with overlaying the calculated band structure. The color scale represents the photoelectron intensity, and gray (purple) dashed curves the original (back-folded) bands. Two surface bands, S_1 and S_2, and their back-folded bands, S_1^{bf} and S_2^{bf}, are marked. (c) SARPES intensity images taken with the region including S_2 and S_2^{bf} bands near E_F surrounded by a thin rectangle in (b). The y-spin polarization component is detected. The two-dimensional color scale represents both the photoelectron intensity and the spin polarization. (d) The x, y, and z components of the spin-resolved spectra in the region marked as l_1 at $K'_{SiC}{}^{bf}$ of S_1^{bf} band in (b).

ably explained by the symmetry while the Rashba-type band crossing is not expected. Using our spin- and angle-resolved photoelectron spectroscopy (SARPES) with three-dimensional spin detection [4] and He Iα (hν ~ 21.22 eV) radiation, both the Zeeman-type and Rashba-type spin splits are confirmed at the K (K') point as shown in Fig. 1(b-d). [4] The surface band S_2 near E_F exhibits a Rashba type inconsistently with the lattice symmetry, while the surface band S_1 around 1.5 eV below E_F is the Zeeman type as expected. It should be noted that the photoelectron intensity for the back-folded band around the K' point due to the graphene-lattice scattering is stronger than that of the original one around the K point in the present experiment conditions.

We have investigated the origin of the two types in the Sn TLAL by evaluating the spin-resolved band structure and charge distribution for the spin-split bands using density functional theory calculations. The directions of the spin polarization are well reproduced by the calculation as in Fig. 2(a,b). The calculated charge distribution of the Rashba-type (Zeeman-type) band at the K point, shown in Fig. 2(c,d), corresponds to a C_{3v} (C_3) symmetry at the K point. Theoretically, the C_{3v} symmetry allows the Rashba-type band crossing regardless of the existence of the time reversal symmetry. [1] The symmetry of the charge density distribution, which is still a consequence of the crystal field potential for the electrons, is a key to understand the nature of the spin splitting due to SOI.

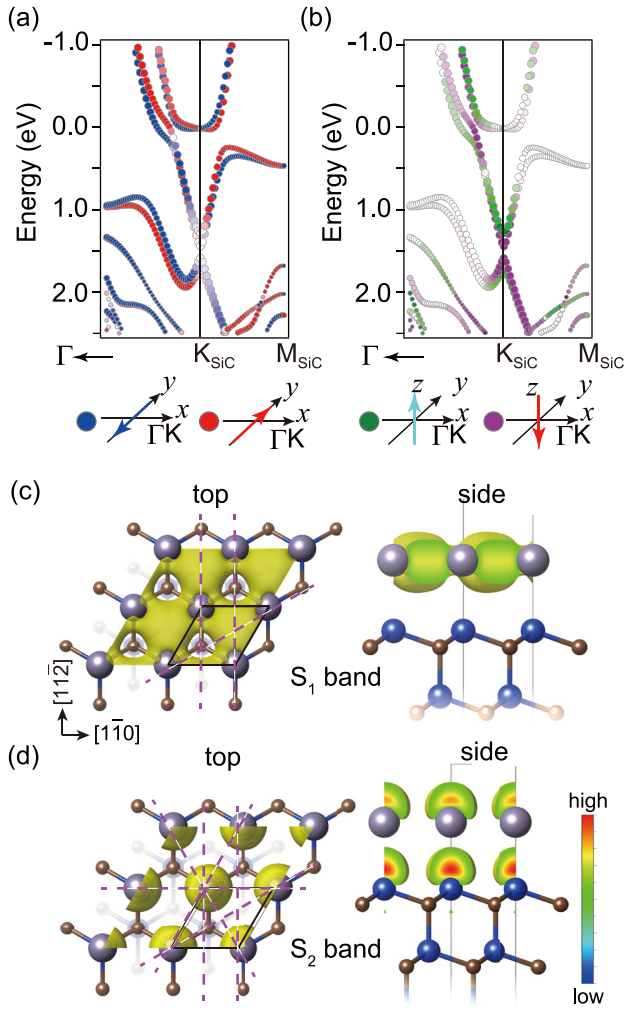

Fig. 2. (a,b) Spin polarization in the y (a) and z (b) directions for the bands around K_{SiC}, where the opposite spin directions are indicated by blue-red and green-purple colors, respectively. The diameter of the circles is proportional to the total contribution of Sn 5s and 5p. (c,d) Charge density distributions for the Zeeman-like spin-split band of S_1 (c) and the Rashba-like spin-split band of S_2 (d) at the K_{SiC} point. Left (right) panels represent top (side) views. In the left panels, the solid parallelograms show the unit cell of Sn/SiC(0001)-(1 × 1). The dashed lines indicate the mirror planes of the charge density distribution.

References

[1] T. Oguchi and T. Shishidou, J. Phys. Condens. Matter **21**,092001 (2009).
[2] S. Hayashi *et al*., Appl. Phys. Express **11**, 015202 (2018).
[3] K. Yaji *et al*., Phys. Rev. Lett. **122**, 126403 (2019).
[4] K. Yaji *et al*., Rev. Sci. Instrum. **87**, 053111 (2016).

Authors

K. Yaji, A. Visikovskiy[a], T. Iimori, K. Kuroda, S. Hayashia, T. Kajiwara[a], S. Tanaka[a], S. Shin, and F. Komori

[a]Kyushu University

Advanced First-Principles Simulation of Electrochemical Interfaces

S. Kasamatsu, I. Hamada, and O. Sugino

Electrochemical interfaces have long been attracting attention as an environment for the interconversion of chemical and electric energies, but the first-principles simulation is not yet sufficiently matured because of the difficulties in (i) achieving the accuracy required for the reliable prediction and (ii) modeling the electric double layers within the density functional theory (DFT). As a step for overcoming, we studied accuracy of the random phase approximation (RPA) for the exchange and correlation (xc) of electrons and then developed an *ab initio* Monte Carlo method suitable for sampling the distribution of defects in an electrode.

Hydrogen (H) on a platinum (Pt) surface, H/Pt(111), is a typical benchmarking system for which many theoretical and experimental studies exist, but controversies still remain even for the H adsorption problem: H is presumed to adsorb on the fcc site based on indirect experiments and the conventional DFT simulations, while there exist several reports that signal from the top site can be observed spectroscopically. Since the conventional DFT, which is based on the semilocal approximation for the xc potential, was shown inaccurate for the sorption problem on Pt(111), we have tried to use more advanced xc potential called RPA [1]. The result of the calculation accurately reproduced the experimental adsorp-

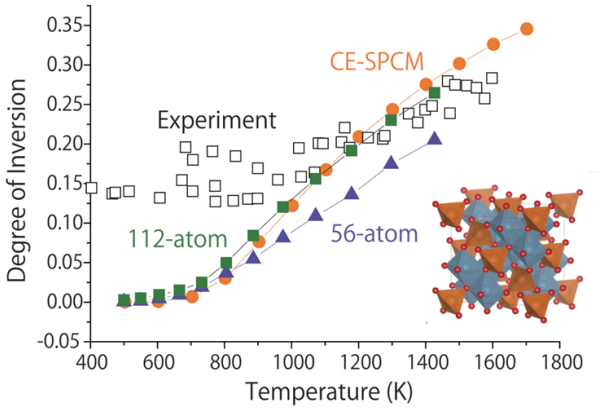

Fig. 1. Plot of the degree of conversion versus the temperature (T) and the $MgAl_2O_4$ spinel structure (inset). Our calculation using 112-atom and 56-atom cells well reproduced the previous simulation based on a cluster expansion model (CE-SPCM) in the whole range of T and also the neutron experiment at higher T. First-principles sampling for solids has thus made feasible.

tion energy although conventional DFT considerably overestimates it. Contrary to the conventional DFT, the DFT-RPA predicts that difference in the energy between the fcc and top sites is on the order of thermal energy at room temperature, i.e. $k_B T_{room}$, suggesting coexistence of the fcc and atop hydrogens. This renewed picture on the H adsorption explains why signal from the top site may be observed. We believe this is an important step for true microscopic understanding of the hydrogen evolution reaction, which is one of the most important fuel-cell reactions.

The fuel-cell reaction occurs efficiently on the Pt electrode but the efficiency needs further improvement to meet the demand of future technology. In this context, oxide electrode (TiO_2 or ZrO_2) has attracted considerable attention as a beyond Pt material. By introducing impurities and oxygen vacancies, the oxides are made active for the fuel-cell reactions. Theoretically, however, it has been extremely difficult to model this system by sampling the distribution of defects for appropriate description of the space charge layer; this is because of the large barrier existing between different configurations of defects. The *ab initio* molecular dynamics (MD) simulation is an established method for the sampling but is generally inadequate for solids. In this context, we have developed an *ab initio* Monte Carlo (MC) method of replica exchange type, which runs very efficiently on massively parallel supercomputers. Our benchmark calculation on $MgAl_2O_4$ spinel shows that the degree of inversion, or the ratio of Al ions on Mg sites, is successfully sampled in the temperature range studied [2] (Fig. 1). This is considered as an important step for elucidation of the reason why the oxides so effectively activate the fuel-cell reactions.

References

[1] L. Yan, Y. Sun, Y. Yamamoto, S. Kasamatsu, I. Hamada, and O. Sugino, J. Chem. Phys. **149**, 164702 (2018).
[2] S. Kasamatsu and O. Sugino, J. Phys.: Condensed Matter, **31**, 085901 (2019).

Authors

L. Yan, Y. Yamamoto, S. Kasamatsu[a], O. Sugino, Y. Sun[b], I. Hamada[c]
[a]Yamagata University
[b]National Institute for Materials Science
[c]Osaka University

Interfacial Hydrogen Bonding in Proton-Electron Concerted 2D Organic Bilayer on Au Substrate Probed by Soft X-Ray Spectroscopy

S. Yamamoto, H. S. Kato, and I. Matsuda

Recent developments in the molecular design of organic materials have uncovered a variety of novel functional properties. One of them is the coupling of proton dynamics and electrical conductivity, which can only be achieved in 3D organic crystals. However, reduction of dimensionality to 2D is essential in organic electronics application. In the functional materials group at ISSP, we aim to realize a 2D organic bilayer with a novel "proton-electron" functionality on a solid surface.

In this study [1], we prepared and characterized a 2D organic bilayer with "proton-electron" concerted functionality on a solid surface. A "proton-electron" concerted organic molecule, catechol-fused bis(methylthio)tetrathiafulvalene (H_2Cat-BMT-TTF), was deposited onto an imidazole-terminated alkanethiolate self-assembled monolayer (Im-SAM) on a Au surface (Fig. 1). In our previous study [2], the OH stretching vibrational modes of H_2Cat-BMT-TTF in the IR spectra showed a large red shift and substantial broadening upon adsorption on Im-SAM, indicating that the OH groups of H_2Cat-BMT-TTF act as the H^+ donor sites. However, the counterpart H^+ acceptor sites was not identified due to an overlap of vibrational peaks. Using near edge X-ray absorption fine structure (NEXAFS) spectroscopy, we succeeded in elucidating the nature of H-bonding at the H^+ acceptor side (*i.e.*, Im-SAM) because N atoms exist only in the Im-SAM layer.

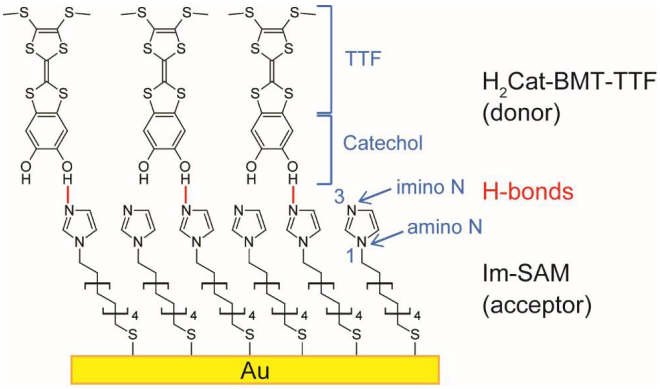

Fig. 1. Schematic structure of organic bilayer of H_2Cat-BMT-TTF and Im-SAM on Au. H_2Cat-BMT-TTF consists of catechol and tetrathiafulvalene (TTF). Im-SAM has two kinds of N atoms: imino N (N3) and amino N (N1). H-bonds are formed between the imino N atoms in Im-SAM (H^+ acceptor layer) and OH groups in H_2Cat-BMT-TTF (H^+ donor layer).

N K-edge NEXAFS spectra of Im-SAM on Au before and after adsorption of H_2Cat-BMT-TTF are shown in Fig. 2. NEXAFS experiments were carried out at soft X-ray beam-line BL07LSU of SPring-8. For Im-SAM on Au, two sharp peaks are observed at 400.0 and 401.8 eV, which are ascribed to the N 1s→1π* transition of the imino N (N3) and amino N (N1) atoms, respectively, of the imidazole ring in Im-SAM. Upon adsorption of H_2Cat-BMT-TTF, the π* peak of imino N (N3) shifts from 400.0 to 400.3 eV, while that of amino N (N1) remains at the same energy. The energies of the π* peaks in NEXAFS are sensitive probes of local chemical environments of specific atoms. The energy shift of the π* peak of imino N (N3) suggests that the local chemical environment of imino N is changed by intermo-

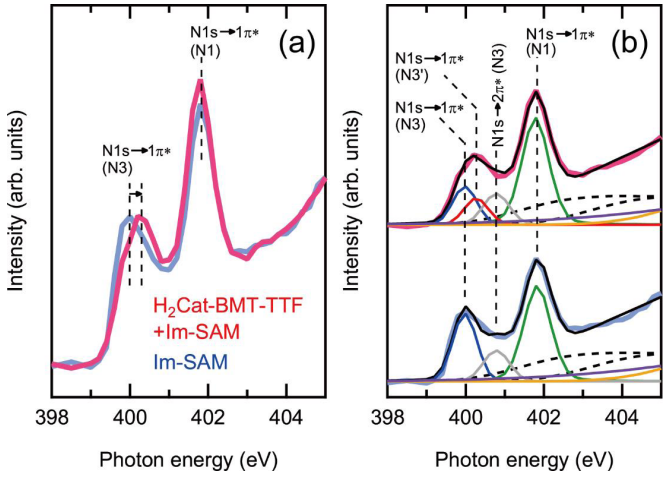

Fig. 2. N K-edge NEXAFS spectra of Im-SAM on Au before and after adsorption of H_2Cat-BMT-TTF. (a) Raw data and (b) raw data with peak fitting results.

lecular H-bonding with H_2Cat-BMT-TTF. The H-bonding configuration between H_2Cat-BMT-TTF and Im-SAM can be discussed based on the quantitative analysis of the coverage of each molecule. The peak fitting of N K-edge NEXAFS spectra in Fig. 2(b) reveals that the coverage of H-bonded Im-SAM is 0.41 ML. This matches the coverage of H_2Cat-BMT-TTF (0.4 ML), which was estimated by X-ray photoelectron spectroscopy in our previous study [2]. This indicates that H_2Cat-BMT-TTF and Im-SAM forms H-bonds in one to one fashion (Fig. 1).

In conclusion, the complete picture of H-bonding in the present organic bilayer was obtained; H-bonds form between the imino N atoms (H^+ acceptor sites) of Im-SAM and the OH groups (H^+ donor sites) of H_2Cat-BMT-TTF. The present work is a steady step toward the realization of 2D organic functional materials, and the experimental methods adopted herein will serve as powerful tools for the detection of their functions.

References

[1] S. Yamamoto, H. S. Kato, A. Ueda, S. Yoshimoto, Y. Hirata, J. Miyawaki, K. Yamamoto, Y. Harada, H. Wadati, H. Mori, J. Yoshinobu, and I. Matsuda, e-J. Surf. Sci. Nanotechnol. **17**, 49-55 (2019).

[2] H. S. Kato, S. Yoshimoto, A. Ueda, S. Yamamoto, Y. Kanematsu, M. Tachikawa, H. Mori, J. Yoshinobu, and I. Matsuda, Langmuir **34**, 2189 (2018).

Authors

S. Yamamoto, H. S. Kato[a], A. Ueda, S. Yoshimoto, Y. Hirata, J. Miyawaki, K. Yamamoto, Y. Harada, H. Wadati, H. Mori, J. Yoshinobu, and I. Matsuda

[a]Osaka University

Structural, Magnetic, and Transport Properties of Novel Quaternary Compounds RRu$_2$Sn$_2$Zn$_{18}$ (R = La, Pr, and Nd)

K. Wakiya, I. Umehara, and Y. Uwatoko

Cubic Pr-based intermetallic compounds are expected to show various fascinating phenomena arising from multipole degrees of freedom, when the crystal electric field (CEF) ground state of Pr^{3+} ion is the non-Kramers Γ_3 doublet. This is because the Γ_3 doublet possesses not a magnetic dipole but electric quadrupoles and a magnetic octupole. Recently, PrT_2X_{20} (T: Transition metal, X = Zn, Al) with the non-Kramers doublet ground state have attracted much attention because they exhibit a coexistence of superconductivity with quadrupole ordering [1-4]. In addition, they exhibit a non-fermi liquid behavior in the electrical resistivity and specific heat [1-4]. It is theoretically suggested that the non-Fermi liquid behavior is caused by the hybridization of quadrupoles with conduction electrons [5]. However, in order to increase our understanding of these phenomena, it is still crucial to find a new Pr compound with the Γ_3 doublet ground state because the number of such compound is limited.

We recently focused on the isostructural compound PrRu$_2$Zn$_{20}$ which shows a structural transition at T_S = 138 K [6]. PrRu$_2$Zn$_{20}$ shows no quadrupole ordering because the CEF ground state doublet is split into two singlets as a result of the site symmetry lowering at the structural transition. In PrT_2Zn$_{20}$, there are three distinct Zn sites: 16c, 48f, and 96g. Among these, Zn atoms at the 16c site [Zn(16c)] is encapsulated by an R_2Zn$_{12}$ cage as shown in the inset of Fig. 1(a). A first principles calculation suggested that the large

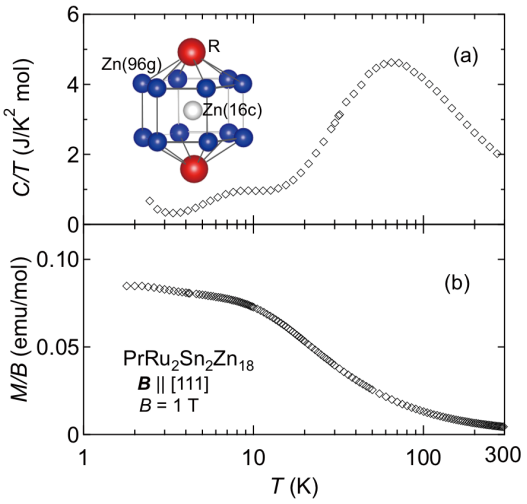

Fig. 1. (a) specific heat divided by temperature C/T and (b) magnetic susceptibility χ (= M/B)of PrRu$_2$Sn$_2$Zn$_{18}$. The inset of (a) shows the Pr$_2$Zn$_{12}$ cage surrounding the Zn atom at the 16c site [Zn(16c)]. In PrRu$_2$Sn$_2$Zn$_{18}$, Zn atoms at the 16c site are fully replaced by Sn atoms.

cage space of R_2Zn$_{12}$ cage induces the structural transition [7]. For RT_2X_{20} (R: Rare earth, T: Transition metal, X = Zn, Al), the cage space is evaluated by subtracting the atomic radius of the caged atom from the average distance between the atoms forming the cage and the caged atom [8]. Recently, in isostructural RT_2Zn$_{20}$ (R = La-Nd, T = Co and Fe), it was reported that Zn(16c) can be fully replaced by the Sn atom [9]. This suggests that the structural transition in PrRu$_2$Zn$_{20}$ can be suppressed by the Sn substitution because the cage space of the Pr$_2$Zn$_{12}$ cage is reduced by introducing the Sn atom with a larger atomic radius into the 16c site. In this study, we synthesized Sn-substituted PrRu$_2$Zn$_{20}$ using self-flux and melt growth methods in order to obtain a new cubic Pr-based compound.

The single-crystal x-ray structural analysis for obtained samples revealed that the Sn atoms selectively occupy the 16c site. Thus, the chemical formula of the obtained sample can be described as PrRu$_2$Sn$_2$Zn$_{18}$. Figure 1(a) shows the specific heat divided by temperature, C/T, of PrRu$_2$Sn$_2$Zn$_{18}$. No anomaly due to a structural transition is observed in C/T, suggesting that PrRu$_2$Sn$_2$Zn$_{18}$ remains cubic even at low temperatures. A broad peak at around 8 K is probably attributed to a Schottky peak due to the CEF splitting. Below 3 K, C/T increases with decreasing temperature, implying that the magnetic entropy is released even below 3 K. Figure 1 (b) shows the magnetic susceptibility χ of PrRu$_2$Sn$_2$Zn$_{18}$. Below 10 K, χ shows a Van-Vleck paramagnetic behavior, indicating that the CEF ground state of PrRu$_2$Sn$_2$Zn$_{18}$ is non-magnetic. Since the Pr site has cubic symmetry, the J multiplet of Pr ion with a total angular momentum of J = 4 split into four multiplets; nonmagnetic Γ_1 singlet and Γ_3 doublet, and magnetic Γ_4 and Γ_5 triplets. Considering that the magnetic entropy is released even below 3 K, the CEF ground state of PrRu$_2$Sn$_2$Zn$_{18}$ should be a nonmagnetic Γ_3 doublet.

In conclusion, we have grown a new quaternary compound PrRu$_2$Sn$_2$Zn$_{18}$. The structural transition in PrRu$_2$Zn$_{20}$ can be suppressed by the Sn substitution. The magnetization and specific heat measurements revealed that the CEF ground state of PrRu$_2$Sn$_2$Zn$_{18}$ is probably a Γ_3 doublet. Therefore, PrRu$_2$Sn$_2$Zn$_{18}$ is a promising material for studying the exotic phenomena arising from the multipole degrees of freedom.

References
[1] T. Onimaru *et al*., Phys. Rev. Lett. **106**, 177001 (2011).
[2] A. Sakai *et al*., J. Phys. Soc. Jpn. **81**, 083702 (2011).
[3] K. Matsubayashi *et al*., Phys. Rev. Lett. **109**, 187004 (2012).
[4] M. Tsujimoto *et al*., Phys. Rev. Lett. **113**, 267001 (2014).
[5] A. Tsuruta and K. Miyake, J. Phys. Soc. Jpn. **84**, 114714 (2015).
[6] T. Onimaru *et al*., J. Phys. Soc. Jpn. **79**, 033704 (2010).
[7] T. Hasegawa *et al*., J. Phys. Conf. Ser. **391**, 012016 (2012).
[8] Z. Hiroi *et al*., J. Phys. Soc. Jpn. **81**, 124707 (2012).
[9] Y. Isikawa *et al*., J. Phys. Soc. Jpn. **84**, 074707 (2015).

Authors
K. Wakiya[a], Y. Sugiyama[a], M. Kishimoto[b], T. D. Matsuda[b], Y. Aoki[b], M. Uehara[a], J. Gouchi, Y. Uwatoko, and I. Umehara[a]
[a]Yokohama National University
[b]Tokyo Metropolitan University

First-Principles Study of Anomalous Nernst Effect on Skyrmion Crystal Chern Insulator

F. Ishii, Y. P. Mizuta, and H. Sawahata

We are interested in how to achieve much higher thermoelectric conversion efficiency by effectively manipulating electron-spin degree of freedom. As one possibility, we have been studying Berry-phase-mediated thermoelectric effects, namely the contribution of the anomalous Hall conductivity (AHC) to thermoelectric power. What we target here is the anomalous Nernst effect (ANE), which is a heat-to-electricity conversion observed in magnetic materials and directly related to AHC. We discussed AHC mainly driven by an effective magnetic field, Berry curvature, induced by spin-orbit coupling and/or spin chirality.

We have so far found from computations on some models that, in the so-called 2D Skyrmion crystal (SkX) phase, where skyrmions are crystallized in two dimensions, the crystal-momentum component of effective magnetic field gives rise to the band structure that could generate large ANE when chemical potential μ is properly tuned [1]. Although this behavior was most clearly confirmed in the simplest model of square SkX with single s-orbital per site, our subsequent computations on more realistic models of transition-metal oxides also showed possible large ANE [2]. A sizable transverse thermoelectric coefficient is predicted to arise, by means of first-principles calculations, in a SkX assumed on EuO monolayer (Fig. 1(a)) where carrier electrons are introduced upon a quantum anomalous Hall insulating phase of Chern number $C = 2$. This encourages future experiments to pursue such an effect.

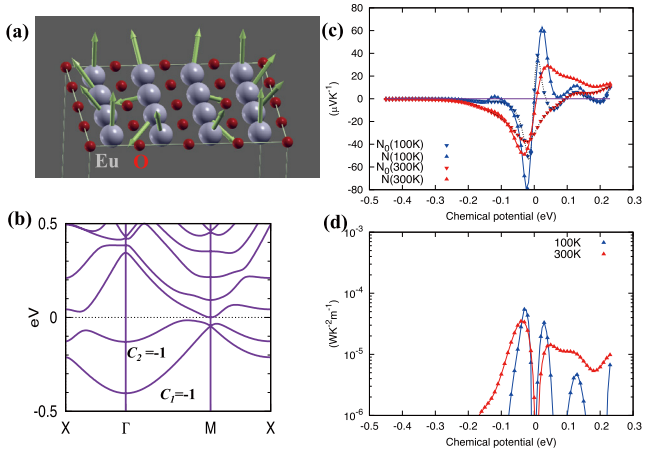

Fig. 1. (a) Calculated spin structures for skyrmion of EuO monolayer model. (b) Calculated band structure, (c) chemical potential dependence of anomalous Nernst coefficients and (d) power factors. Results are shown for different values of temperature 100K and 300K. We assumed the constant relaxation time $\tau = 10$ fs.

Figure 1 (b) shows the band structure of electron-doped EuO monolayer. There is a narrow band gap of ~20 meV between the valence band top and conduction band bottom. The Chern number was calculated by integrating Berry curvatures of Brillouin zone. The occupied two bands with Chern number $C = 2$ are mainly composed of Eu 5d and 6s characters. We have calculated anomalous Nernst coefficients N and pure Nernst coefficients $N_0 \equiv \alpha_{xy}/\sigma_{xy}$ [2] by using semiclassical Boltzmann transport theory with constant relaxation time, $\tau = 10$ fs. The calculated chemical potential dependence of Nernst coefficients N, pure Nernst coefficients and power factor are plotted in Fig 1(c) and (d). The large anomalous Nernst coefficients up to 60 μV/K and power factor up to 70 μW/mK^2 can be obtained.

Such N arises from the coexistence of large longitudinal thermoelectric coefficient and large Hall angle ratio, realized in the vicinity of a narrow band gap with Chern number $C = 2$. This demonstrates a prototype of novel class of new thermoelectric materials utilizing the nanoscale topological spin textures, motivating further studies including relevant experiments. We concluded that the SkX and narrow-gap Chern insulators could be candidate materials for thermoelectric applications.

References
[1] Y. P. Mizuta and F. Ishii, Sci. Rep. **6**, 28076 (2016).
[2] Y. P. Mizuta, H. Sawahata, and F. Ishii, Phys. Rev. B **98**, 205125 (2018).

Authors
F. Ishii[a], Y.P. Mizuta[b], and H. Sawahata[a]
[a]Kanazawa University
[b]Osaka University

Heavy-Fermion State in Valence-Fluctuating Antiferromagnetic Compound $EuPt_2Si_2$ under High Magnetic Field and High Pressure

T. Takeuchi, Y. Ōnuki, and T. Kida

$EuPt_2Si_2$ crystallizes in the $CaBe_2Ge_2$-type tetragonal crystal structure and is known as a valence-fluctuating compound. From the $\chi(T)$ measurement of polycrystalline samples, it is found that $EuPt_2Si_2$ orders antiferromagnetically at $T_N = 15$ K. $\chi(T)$ at high temperatures follows the Curie-Weiss law with an effective magnetic moment of $\mu_{eff} = 7.7\ \mu_B$/Eu, indicating that the Eu ions are essentially divalent. Here, μ_{eff} for the Eu^{2+} free-ion is 7.94 μ_B/Eu. On the other hand, an unusual broadening of the Mössbauer resonance line width is observed below about 100 K, suggesting that the valence is fluctuating and already deviates slightly from divalent to trivalent at room temperature. One of the intriguing findings for $EuPt_2Si_2$ is the -ln$T$ dependence of $\rho(T)$ below $T \simeq 100$ K. In addition, the magnetic entropy of $S_{mag} \simeq 0.6R\ln 8$ below T_N and the strongly enhanced $\gamma \simeq 200$ mJ/(K^2·mol) suggest that a heavy-fermion state is realized at low temperatures in $EuPt_2Si_2$.

To obtain more insight into the heavy-fermion features in $EuPt_2Si_2$, we grew single crystals of this compound and studied the effects of a magnetic field as well as pressure on its magnetic properties.

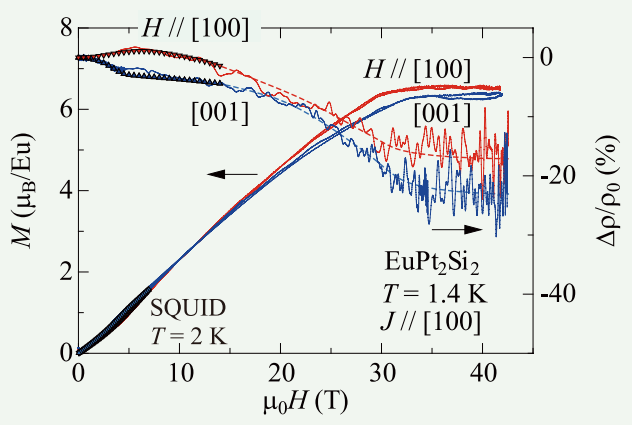

Fig. 1. High-field magnetization curves $M(H)$ (left-hand scale) and relative changes in the magnetoresistance $\Delta\rho/\rho_0$ for J // [100] (right-hand scale) in magnetic fields applied parallel to the [100] and [001] directions at 1.4 K. The $M(H)$ data below 7 T were measured in static magnetic fields using a SQUID magnetometer at 2 K. The $\Delta\rho/\rho_0$ curves below 14 T were measured using a superconducting magnet. Broken lines for $\Delta\rho/\rho_0$ at high magnetic fields are guides to the eye.

The single crystal of $EuPt_2Si_2$ shows two antiferromagnetic transitions at T_{N1} = 21 K and T_{N2} = 16 K. The -ln$T$ dependence of $\rho(T)$ was observed in the temperature range from T_{N1} to about 100 K, as observed in polycrystals. The effect of magnetic field on the -ln$T$ dependence of $\rho(T)$ is found to be very weak, with $\Delta\rho/\rho_0$ of only ~0.1% at μ_0H = 8 T. Even at μ_0H = 40 T, which was produced using a pulsed magnet, $\Delta\rho/\rho_0$ amounted to only -20%, as shown in Fig. 1. These results suggest that the Kondo-like behavior of $EuPt_2Si_2$ is rather stable against the application of magnetic field, which is in contrast to the Ce-based heavy-fermion compounds.

On the other hand, the pressure markedly shifts the -ln T dependence of $\rho(T)$ to higher temperatures, and T_{N1} is gradually decreased and suppressed to zero above $P \simeq 4$ GPa, as indicated in Fig. 2. From the comparison of the observed magnetic, electronic, and thermal properties of $EuPt_2Si_2$ with those of the well studied $EuCu_2(Ge_{0.4}Si_{0.6})_2$,[2] the anomalous features observed below 100 K in $\rho(T)$, $S(T)$, and $\Delta V/V$ for $EuPt_2Si_2$ are most likely to be due to the valence fluctuation of the Eu ions. As a future problem, X-ray absorption and Mössbauer experiments are desirable to confirm the temperature dependence of the Eu valence in $EuPt_2Si_2$.

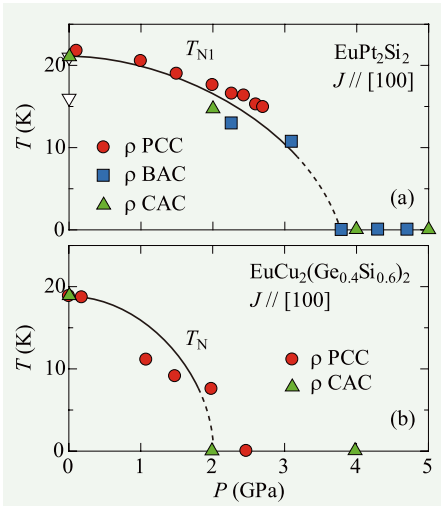

Fig. 2. Comparison of the P–T phase diagrams for $EuPt_2Si_2$ and $EuCu_2(Ge_{0.4}Si_{0.6})_2$, cited from Ref. [2]. The P–T phase diagram for $EuCu_2(Ge_{0.4}Si_{0.6})_2$ was obtained by the resistivity measurements for J // [100] under pressures. PCC, BAC, and CAC denote piston cylinder cell, Bridgman anvil cell, and cubic anvil cell.

References

[1] T. Takeuchi *et al.*, J. Phys. Soc. Jpn. **87**, 074709 (2018).
[2] W. Iha *et al.*, J Phys. Soc. Jpn. **87**, 064706 (2018).

Authors

T. Takeuchi[a], T. Yara[b], Y. Ashitomi[b], W. Iha[b], M. Kakihana[b], M. Nakashima[c], Y. Amako[c], F. Honda[d], Y. Homma[d], D. Aoki[d], Y. Uwatoko, T. Kida[a], T. Tahara[a], M. Hagiwara[a], Y. Haga[e], M. Hedo[b] T. Nakama[b], and Y. Ōnuki[b]

[a]Osaka University
[b]University of the Ryukyus
[c]Shinshu University
[d]Tohoku University
[e]Japan Atomic Energy Agency

Magnetoelectric Behavior from Square Cupola Magnetic Units in High Magnetic Field

K. Kimura, Y. Kato, and A. Miyake

A particular class of magnetic order with broken space-inversion and time-reversal symmetries has recently attracted considerable interest because it can exhibit symmetry-dependent unique phenomena, such as linear magnetoelectric (ME) effects and associated nonreciprocal optical responses. In exploring such a magnetic order, a material composed of inversion asymmetric magnetic units is fascinating, because structural asymmetry of the unit may stabilize a nontrivial non-coplanar spin arrangement due to asymmetric Dzyaloshinskii-Moriya (DM) interactions, which would lead to various magnetoelectric responses. Recently, we have synthesized new antiferromagnetic insulators $A(TiO)Cu_4(PO_4)_4$ (A = Ba, Sr, and Pb), which consists of Cu_4O_{12} convex-shaped magnetic units known as square cupola [Inset of Fig. 1(a)] [1-4]. Their crystal structure belongs to a tetragonal space group $P42_12$ and is characterized by a layered arrangement of Cu_4O_{12} square cupolas. Interestingly, neutron diffraction study [2] reveals that below the antiferromagnetic ordering temperature T_N, four Cu^{2+} spins of each square cupola forms a magnetic quadrupole moment, which, along with magnetic monopole and toroidal moments, is known as one of cluster multipole moments that satisfy the symmetry condition for the linear ME effect. Indeed, we observed a magnetic-field-induced electric polarization in the Pb system and a sharp dielectric anomaly at T_N in the Ba and Sr systems. (The difference originates from a stacking manner of magnetic layers: the quadrupole moments stack ferroically in the Pb system, while antiferroically in the Ba

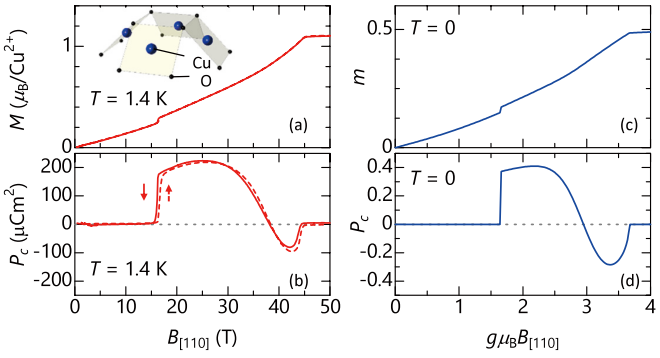

Fig. 1. Magnetic field dependence of magnetization (M) and electric polarization along the c axis (P_c) obtained in (a) and (b) experiments and (c) and (d) theoretical calculations for $Pb(TiO)Cu_4(PO_4)_4$ (see Ref. [5] for details). The magnetic field was applied along the [110] axis. The inset of (a) shows a Cu_4O_{12} square cupola magnetic unit.

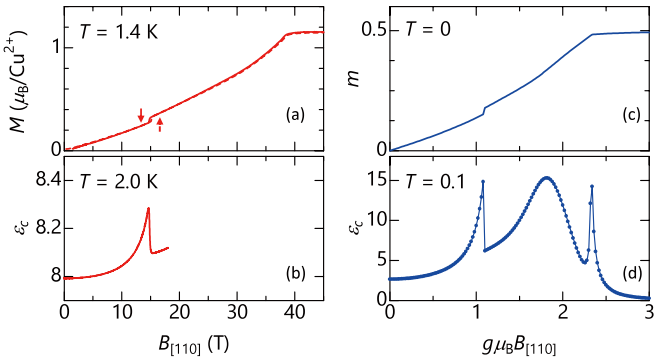

Fig. 2. Magnetic field dependence of magnetization (M) and dielectric constant along the c axis (ε_c) obtained in (a) and (b) experiments and (c) and (d) theoretical calculations for $Sr(TiO)Cu_4(PO_4)_4$ (see Ref. [6] for details). The magnetic field was applied along the [110] axis.

and Sr systems.) These results demonstrate that magnetic square cupolas are promising ME-active structural units in the low magnetic field (B) quadrupole phase. However, their ME activity in a B-induced phase, which appears commonly in these materials above 10 T, has not been elucidated. In this study, we have investigated ME properties in the B-induced phases of the Pb [5] and Sr [6] systems.

Figures 1(a) and 1(b) show a B-dependence of electric polarization along the c axis (P_c) in the Pb system, together with magnetization along the [110] axis ($M_{[110]}$) for comparison. The B along the [110] direction ($B_{[110]}$) was applied with use of a pulsed magnet. It is observed that P_c develops upon the onset of the B-induced phase at 16.4 T. A clear PE hysteresis loop was observed at steady B of 18 T, confirming the ferroelectric nature. Moreover, $P_{[001]}$ shows a B-induced sign reversal around 35 T. On the basis of the space group $P4_212$ in the paramagnetic phase and the existence of finite $M_{[110]}$ and P_c, a possible maximal magnetic point group of the $B_{[110]}$-induced phase is $2'$, which supports a cluster multipole moment composed of toroidal and magnetic moments. Contrary to the Pb case, no finite P_c was observed in the $B_{[110]}$-induced phase of the Sr system. Instead, as shown in Figs. 2(a) and 2(b), a sharp peak in the dielectric constant along the [001] axis (ε_c) appears at the transition field of ~15.0 T. (ε_c was measured up to 18 T using a superconducting magnet.) Considering the antiferroic stacking of magnetic layers at a low B quadrupole phase, the $B_{[110]}$-induced phase of the Sr system is expected to be antiferroelectric with a staggered electric polarization along the c axis.

To understand the origin for the experimental results, we have constructed a spin-1/2 effective model, in which a DM interaction between neighboring spins due to convex geometry is taken into account. As shown in Figs. 1(c) and 2(c), this model well reproduces the experimental M curves in both systems, which strongly supports the validity of our model analysis. Next, we evaluated the $B_{[110]}$ dependence of P_c in the Pb system and ε_c in the Sr system on the basis of the so-called exchange striction mechanism. As shown in Figs. 1(c) and 2(c), the calculated P_c and ε_c are qualitatively in good agreement with experimental results. The analysis thus indicates that the exchange striction plays a prime role for the ME behavior from Cu_4O_{12} square cupolas in the $B_{[110]}$-induced phase. Moreover, a cluster multipole decomposition was applied to the calculated spin arrangement of square cupolas. The result shows that both toroidal and quadrupole moments become finite in each magnetic layer. This can explain the ferroelectricity and antiferroelectricity along the c axis induced by $B_{[110]}$.

The present results thus demonstrate that Cu_4O_{12} square cupolas are promising ME active structural units in a broad range of a magnetic field. Distinct types of ME-active multipole moments can appear in different phases. The convex shaped geometry of Cu_4O_{12} square cupolas plays an important role for the onset of such ME active multipole moments. This implies that not only the square cupola unit, but also other types of convex-shaped structural units are worth to be explored for new magnetoelectric materials.

References
[1] K. Kimura *et al.*, Nat. Commun. **7**, 13039 (2016).
[2] Y. Kato *et al.*, Phys. Rev. Lett. **118**, 107601 (2017).
[3] P. Babkevich *et al.*, Phys. Rev. B **96**, 214436 (2017).
[4] K. Kimura *et al.*, Phys. Rev. B **97**, 134418 (2018).
[5] K. Kimura *et al.*, Phys. Rev. Mater. **2**, 104415 (2018).
[6] Y. Kato *et al.*, Phys. Rev. B **99**, 024415 (2019).

Authors
K. Kimura[a], Y. Kato[b], K. Yamauchi[c], A. Miyake, M. Tokunaga, A. Matsuo, K. Kindo, M. Akaki, M. Hagiwara, S. Kimura[d], M. Toyoda[e], Y. Motome[b], and T. Kimura[a]
[a]Department of Advanced Materials Science, University of Tokyo
[b]Department of Applied Physics, The University of Tokyo
[c]ISIR-SANKEN, Osaka University
[d]Institute for Materials Research, Tohoku University
[e]Tokyo Institute of Technology

Electric Dipole Spin Resonance in the Interacting Quantum Spin Dimer System $KCuCl_3$

S. Kimura, M. Matsumoto, and M. Akaki

The observation of optical transition from spin singlet to triplet states by means of high frequency electron spin resonance (ESR) measurements is known as an advantageous tool to investigate the energy spectrum of quantum spin gap systems, such as a Haldane system or a spin ladder, in high accuracy. The transition has been reported for many spin gapped system, for instance $Ni(C_2H_8N_2)_2NO_2ClO_4$ (NENP), $CuGeO_3$ and $SrCu_2(BO_3)_2$. However, the singlet-triplet transition is, in principle, forbidden in magnetic dipole transition, and therefore the origin of its finite transition probability is not so clear at the moment.

Here we report on our recent high frequency ESR study on the S = 1/2 interacting dimer system $KCuCl_3$. By measuring polarization dependence of the ESR signal, we have clarified that the singlet-triplet transition in this compound is due to the electric dipole transition [1]. In $KCuCl_3$, spin dimers composed of two Cu^{2+} spins form a three dimensional network in the monoclinic crystal. Reflecting this dimer structure, the ground state of this compound is the spin singlet state, and does not order down to the lowest temperature. From the previous measurements, two sets of the singlet-triplet transitions were observed [2]. The two sets of the singlet-triplet transitions are due to two kinds of the crystallographically different dimers in the unit cell of $KCuCl_3$, which gives rise to superposition of two kinds of the triplet excitation modes in the momentum space. To determine the selection rules of the singlet-triplet transition, we have performed the high frequency ESR measurements by illuminating linearly polarized electromagnetic wave to the sample.

Figure 1 shows the ESR signals from the singlet-triplet transition in $KCuCl_3$ in external magnetic fields parallel to the b axis. Our experiment showed that both the lower and

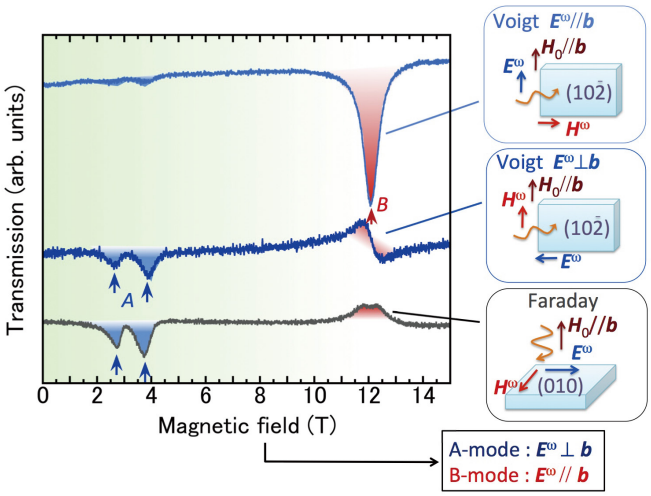

Fig. 1. ESR signals of the singlet-triplet transitions in $KCuCl_3$, observed in the Faraday and Voigt configurations. In the measurements in the Voigt configuration, linearly polarized electromagnetic wave is illuminated to the sample. The ESR signals *A* and *B* come from the higher and lower triplet excitation modes, respectively. The experimental result shows that both signals are electrically driven, and directions of the oscillating electric fields, which couples to *A* and *B*, are orthogonal each other.

higher energy triplet modes *A* and *B* couple with oscillating electric fields of the electromagnetic wave. Furthermore, the directions of the oscillating electric fields, which couple to the *A* and *B* modes, are orthogonal each other. These behaviors are explained by the spin dependent electric polarization. Recent studies for magntoelectric multiferroic materials revealed that the vector spin chilarity $\boldsymbol{S}_i \times \boldsymbol{S}_j$, which is an outer product of neighboring spin, induces an electric polarization $\boldsymbol{P}$, as $\boldsymbol{P} = \tilde{C}\,(\boldsymbol{S}_i \times \boldsymbol{S}_j)$, where $\tilde{C}$ is a second rank tensor. Coupling between this $\boldsymbol{P}$ and the oscillating electric fields $Ee^{-i\omega t}$ can be regarded as a dynamical Dzyaloshinsky-Moriya (DM) interaction, oscillating with an angular frequency ω. Because DM interaction has finite matrix elements between spin singlet and triplet states, the electric dipole transition between these states can occur. By taking into account the two-fold helical axis between the two dimers, the observed characteristic selection rule of the singlet-triplet transition is also explained. The electric polarization, generated by $\boldsymbol{S}_\mathrm{i} \times \boldsymbol{S}_\mathrm{j}$, can appear regardless of the local structural symmetry between the two spin sites. Therefore, electric dipole spin resonance by the spin-dependent electric polarization is universal for spin gapped systems. It is possible that the singlet-triplet transitions that were previously observed in various spin gapped materials are induced by this polarization mechanism.

References

[1] S. Kimura, M. Matsumoto, M. Akaki, M. Hagiwara, K. Kindo, and H. Tanaka, Phys. Rev. B **97**, 140406 (2018).
[2] H. Tanaka, K. Takatsu, W. Shiramura, T. Kambe, H. Nojiri, T. Yamada, S. Okubo, H. Ohta, and M. Motokawa, Physica B **246-247**, 545 (1998).
[3] H. Katsura, N. Nagaosa, and A. V. Balatsky, Phys. Rev. Lett. **95**, 057205 (2005).
[4] T. A. Kaplan and S. D. Mahanti, Phys. Rev. B **83**, 174432 (2011).

Authors

S. Kimura[a], M. Matsumoto[b], M. Akaki[c], M. Hagiwara[c], K. Kindo and H. Tanaka[d]
[a]Tohoku University
[b]Shizuoka University
[c]Osaka University
[d]Tokyo Institute for Technology

Emergent Transport Phenomena in the Course of Multiple Topological Transitions in $MnSi_{1-x}Ge_x$

N. Kanazawa, Y. Tokura, and M. Tokunaga

Interplay between topological spin textures and conduction electrons produces giant effective magnetic field called emergent magnetic field, leading to various electromagnetic functionalities for next-generation memory devices and energy-harvesting technology. Skyrmion and hedgehog spin structures are representative examples, which show two- and three-dimensional (2D and 3D) topological spin arrangements, respectively. Reflecting their topological properties, distinct emergent field distributions and each characteristic response are realized, i.e., flux-line- and monopole-like behaviors in skyrmion and hedgehog systems.

By synthesizing alloys of skyrmion- and hedgehog-hosting compounds (MnSi and MnGe), we investigate the transformation process between skyrmion and hedgehog spin textures, where new type of topological phase transition is expected. We also perform high-magnetic field measurements on Hall resistivity to unravel the emergent field profiles upon complete unwinding those highly-stable magnetic knots. Precise transport measurements with μΩ-resistance resolusion were achieved by utilizing non-destructive pulse magnets energized by capacitor banks and a flywheel DC generator installed at International MegaGauss Science Laboratory of Institute for Solid State Physics (ISSP).

We have observed three different magnetic phases with varying composition x in $MnSi_{1-x}Ge_x$. As shown in the magnetic phase diagrams (Fig. 1), each magnetic phase exhibits a unique magnetic field value for the transition to ferromagnetic state (approximately 1 T for $0 < x < 0.3$, 10 T for $0.3 < x < 0.7$, and 20 T for $0.7 < x < 1$), which is suggestive of the difference in topological property of the winding spin texture. In particular, we identified a new type of hedgehog lattice in $MnSi_{1-x}Ge_x$ with intermediate composition $x = 0.4 - 0.6$, i.e., at the expected topological magnetic transition between the 2D skyrmion lattice (SkL) and the 3D hedgehog lattice (HL). This magnetic state consists of hedgehogs and anti-hedgehogs aligned in face-centered-cubic positions (Fig. 1). We also revealed emergent field profiles characteristic to each magnetic state as topological Hall effect (Fig. 2). There observed much difference in magnitudes and *H*-dependence, again contrasting the three topological phases.

In conclusion, we demonstrate the transitions among distinct topological spin textures, namely 2D SkL and two classes of 3D HLs, which are simply induced by controlling lattice constant or chemical pressure. The present study

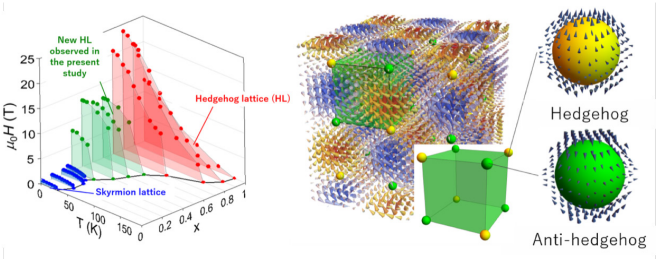

Fig. 1. (left) Variation of magnetic phase diagrams in $MnSi_{1-x}Ge_x$. The three colors represent different topological magnetic phases. (right) Schematic illustration of the new hedgehog lattice state identified in this study.

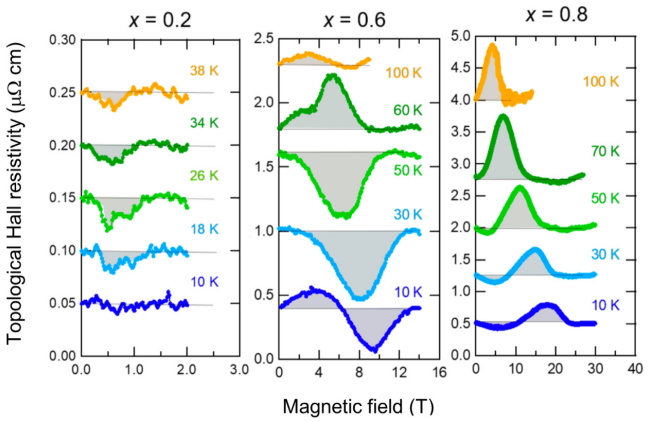

Fig. 2. Representative profiles of topological Hall resistivity for three different magnetic states (x = 0.2 for SkL, x = 0.6 for fcc HL, and x = 0.8 for cubic HL).

suggests a new route for the direct manipulation of the spin-texture topology. Furthermore, the established precise high-field transport measurement technique will contribute to detection of emergent electromagnetic fields appearing as less-dissipative current and concomitant small resistance change.

References

[1] Y. Fujishiro, N. Kanazawa, T. Nakajima, X. Z. Yu, K. Ohishi, Y. Kawamura, K. Kakurai, T. Arima, H. Mitamura, A. Miyake, K. Akiba, M. Tokunaga, A. Matsuo, K. Kindo, T. Koretsune, R. Arita, and Y. Tokura, J. Phys. Soc. Jpn. **75**, 043707 (2006).

Authors

Y. Fujishiro[a], N. Kanazawa[a], T. Nakajima[b], X. Z. Yu[b], K. Ohishi[c], Y. Kawamura[c], K. Kakurai[b,c], T. Arima[b,d], H. Mitamura, A. Miyake, K. Akiba, M. Tokunaga, A. Matsuo, K. Kindo, T. Koretsune[e], R. Arita[a,b], and Y. Tokura[a,b]

[a]Department of Applied Physics, the University of Tokyo
[b]RIKEN Center for Emergent Matter Science (CEMS)
[c]Neutron Science and Technology Center, Comprehensive Research Organization for Science and Society (CROSS)
[d]Department of Advanced Materials Science, the University of Tokyo
[e]Tohoku University

Ferromagnetic-to-Helimagnetic Transition in Cubic Perovskites $Sr_{1-x}Ba_xCoO_3$

H. Sakai, M. Tokunaga, and S. Ishiwata

Helimagnets have recently attracted great interest in terms of fundamental physics and (spin)electronic application, owing to their novel functions that simple ferromagnets have never attained. Typical examples include spin-spiral-driven ferroelectricity in perovskite-type manganites and current-driven motion of magnetic skyrmions in chiral magnets. However, since the helimagnetic order originates from several competing magnetic interactions, its emergence is highly limited by strong constraints on the lattice and spin systems.

Here we report the emergence of helimagnetism out of room-temperature ferromagnetism in simple cubic perovskites $Sr_{1-x}Ba_xCoO_3$ by the negative chemical pressure (Fig. 1). By utilising a high-pressure technique, we have successfully grown a series of single crystals with systematical chemical compositions. With the isotropic lattice expansion by Ba substitution, room-temperature ferromagnetism for $SrCoO_3$ is markedly suppressed, leading to incommensurate helimagnetism, while the simple cubic structure remains intact. High-resolution neutron diffraction the Ba-substituted

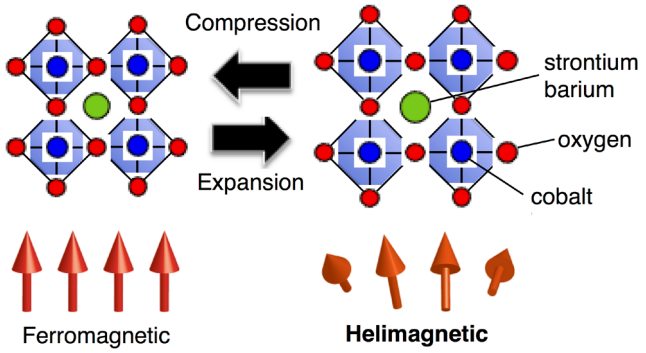

Fig. 1. Schematic illustration of the helimagnetic-ferromagnetic transition driven by the lattice expansion/compression in the cubic perovskite $Sr_{1-x}Ba_xCoO_3$.

compounds has revealed the helimagnetic correlation that evolves towards low temperatures in competition with ferromagnetic one [1].

Figure 2(a) shows the temperature dependence of the magnetisation M at 0.01 T for $Sr_{1-x}Ba_xCoO_3$, measured upon heating after a field cooling process. With increasing x from 0.1 to 0.35, the ferromagnetic Curie temperature T_C decreases systematically from 256 K to 176 K. For x = 0.35, the increase in M below T_C is largely reduced, and instead a clear drop in M upon cooling manifests itself at T_M (~43 K). For x = 0.4, the ferromagnetic transition disappears and the drop in M is more conspicuous. This corresponds to the onset of the helimagnetic correlations as revealed by the neutron diffraction experiments. To check the spin state of Co^{4+} ions upon Ba substitution, we have also measured the field profile of M at the lowest temperature (2–4 K) (Fig. 2(b)). For x = 0.1–0.3 with the ferromagnetic ground state, the M value is saturated above ~2 T, whereas the saturation field is substantially enhanced with increasing x to 0.35, where the helimagnetic instability sets in. The value of M barely saturates at above ~30 T for x = 0.35. From these data, we have found that the saturation moment is almost constant (~2.2–2.5μ_B/Co) with x up to 0.35 in spite of a significant decrease in T_C. The spin state thus appears to remain in a nearly intermediate, i.e., S = 3/2, configuration, which is likely to be strongly hybridised with the ligand hole states (see the inset to Fig. 2(b)).

Our results indicate that the subtle balance among the magnetic interactions can be controlled by the lattice size, i.e., bandwidth, which reflects the strong p-d hybridization inherent in the unusually high-valence Co^{4+} state. The discovery of the helimagnetic order by expanding the simple

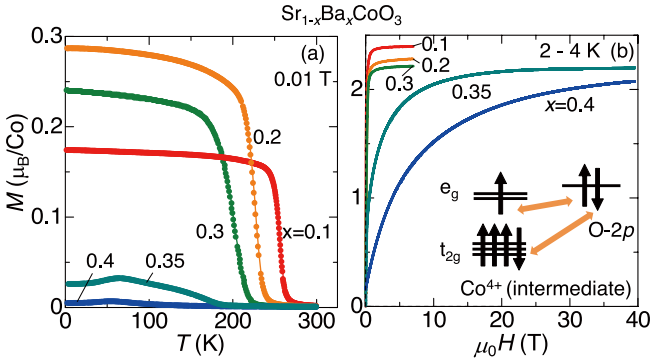

Fig. 2. (a) Temperature (T) profiles of magnetisation (M) at 0.01 T for $Sr_{1-x}Ba_xCoO_3$ ($0.1 \le x \le 0.4$) single crystals. (b) Field dependence of M at the lowest temperature (2-4 K) for x=0.1-0.4. The profiles up to ~40 T were measured with a pulse magnet. Inset shows schematic diagram of intermediate spin configuration of Co^{4+}. L denotes an oxygen ligand hole.

cubic lattice provides a foundation for investigating the properties of many other crystalline materials.

Reference
[1] H. Sakai, S. Yokoyama, A. Kuwabara, J. S. White, E. Canévet, H. M. Rønnow, T. Koretsune, R. Arita, A. Miyake, M. Tokunaga, Y. Tokura, and S. Ishiwata, Phys. Rev. Materials. **2**, 104412 (2018).

Authors
H. Sakai[a,b,c], S. Yokoyama[a], A. Kuwabara[a], A. Miyake, M. Tokunaga, Y. Tokura[a], and S. Ishiwata[a,c]
[a]The University of Tokyo
[b]Osaka University
[c]PRESTO, JST

Magnetic-Field-Induced Kondo Metal State in the Kondo Insulator YbB_{12}

F. Iga, Y. H. Matsuda, and Y. Kohama

The Kondo effect is one of the most intensively studied many-particle correlation effects and induces intriguing phenomena such as heavy fermions and characteristic behaviors of electrons in quantum dots. There are rare materials in which insulating phases appear with development of the Kondo effect at low temperatures and they are termed Kondo insulator. Since most of the compounds with significant Kondo effect are metallic, the origin of formation of the charge gap has been attracting attention for a long time. Application of magnetic field (B) is expected to control the electronic state of the Kondo insulator through the Zeeman effect, and the magnetic field induced insulator-metal (IM) transition actually occurs in the prototypical Kondo insulator YbB_{12} at around 50 T [1]. The properties of the high-field metallic phase have never been well understood because the magnetic field required is rather high, which makes microscopic measurements difficult to perform.

Here we report on specific heat (C_p) measurements of YbB_{12} in high magnetic fields of up to 60 T. The techniques for measurements of specific heat in a pulsed magnetic field have been developed recently [2] and applied to researches of various kinds of materials. We found that the specific heat sharply increases as the IM transition takes place around 50 T. This largely enhanced value of specific heat coefficient (C_p /T) strongly indicates that a large density of state (DOS) emerges at the Fermi energy and the electronic state corresponds to the Kondo metal state with heavy mass quasi particles.

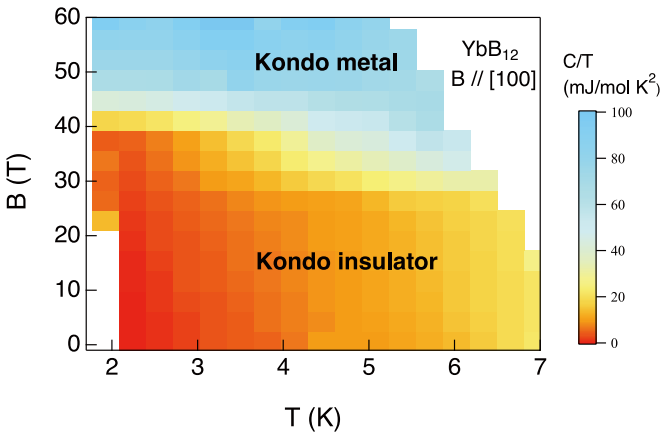

Fig. 1. The plot of the C_p / T in the B-T plain with a color gradient scale. The Kondo metal phase appears in high magnetic fields.

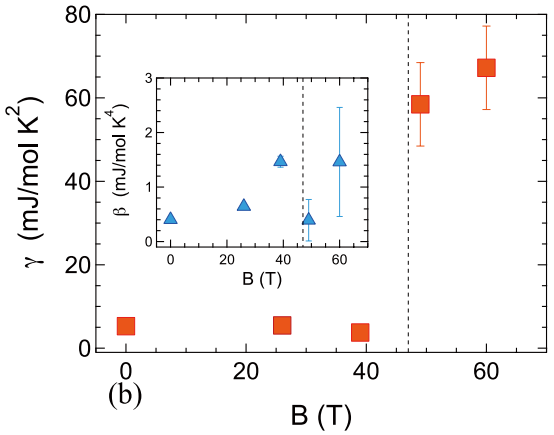

Fig. 2. Sommerfeld coefficient γ is plotted as a function of the magnetic field. The jump of γ to a large value is a direct evidence of appearance of a Kondo metal with heavy mass quasi particles.

Figure 1 shows a color plot image of the C_p /T in the B-T plane. The Kondo metal state is found to appear in higher field region. Using the relation C_p /T = γ + βT^2, where the second term is due to phonon contribution with a constant β, the Sommerfeld coefficient γ is deduced from the temperature variation of C_p. The deduced γ is plotted as a function of the magnetic field in Fig. 2. A similar plot for β is shown in the inset. The vertical dashed lines denote the magnetic field where the IM transition takes place [3]. A distinct increase of γ occurs along with the IM transition, and the γ at a high-field metal phase is 58 mJ/(mol K^2) and 67 mJ/(mol K^2) at 49 T and 60 T, respectively. Although β may also have finite magnetic field dependence, it is relatively smaller than the large field-induced change in γ and can be ignored at low temperatures. It is also interesting to note that the obtained γ is as large as that in Kondo metals that exhibit strong valence fluctuations. For instance, γ is 50 mJ/(mol K^2) in $YbAl_3$ and 130 mJ/(mol K^2) in α-$YbAlB_4$. $YbAl_3$ is one of the typical valence fluctuation compounds, and α-$YbAlB_4$ is the anisotropic heavy fermion compounds with significant valence fluctuations. From the value of γ, it is clearly concluded that the field-induced metal state in YbB_{12} is regarded as a Kondo metal in the valence fluctuation regime [4].

We can evaluate the Kondo temperature T_K in the high-field Kondo metal phase. The entropy S in the field-induced metal can be estimated from the degeneracy W of the magnetic state of 4f electrons in trivalent Yb ions. The ground state of the Yb^{3+} ions in the cubic crystal field in YbB_{12} is Γ_8 and the W is 4. The excited Γ_6 and Γ_7 doublets are almost degenerated and located at a higher energy than Γ_8 by about 23 meV. Since the energy gap (15 meV) collapses due to the Zeeman effect at the transition magnetic field and this energy scale is comparable to the excitation energy of the crystal field splitting (23 meV), the three $\Gamma_{6,7,8}$ states more or less mix each other in high magnetic fields, and thus, the upper limit of W is 8. The S is safely evaluated to be between R ln4 and R ln8, where R is the gas constant. Using the relation $\gamma T_K \sim S$, T_K is deduced to be 172K (for W = 4) and 258 K (for W = 8) at 60 T. The obtained T_K is comparable to that of α-$YbAlB_4$ ($T_K \sim 200$ K).

The theoretical work using dynamical mean field theory [5] predicts the appearance of the Kondo metal phase in high magnetic fields, whose Zeeman energy becomes comparable to the energy gap. According to this calculation, a sharp peak of DOS appears at the IM transition, and the calculated magnetization shows a steep increase at the transition that is in good agreement with the experimentally obtained results. The sharp peak can be considered as the field-induced Kondo

resonance peak. In even greater magnetic fields, the Kondo effect is expected to be sufficiently suppressed. The recent report on the magnetization process in YbB_{12} suggests that the magnetic field for the Kondo breakdown is as high as 120 T [6].

References

[1] K. Sugiyama, F. Iga, M. Kasaya, T. Kasuya, and M. Date, J. Phys. Soc. Jpn. **57**, 3946 (1988).
[2] Y. Kohama, Y. Hashimoto, S. Katsumoto, M. Tokunaga, and K. Kindo, Meas. Sci. Technol. **24**, 115005 (2013).
[3] F. Iga, K. Suga, K. Takeda, S. Michimura, K. Murakami, T. Takabatake, and K. Kindo, J. Phys. Conf. Ser. **200**, 012064 (2010).
[4] T. T. Terashima, Y. H. Matsuda, Y. Kohama, A. Ikeda, A. Kondo, K. Kindo, and F. Iga, Phys. Rev. Lett. **120**, 257206 (2018).
[5] T. Ohashi, A. Koga, S.-i. Suga, and N. Kawakami, Phys. Rev. B **70**, 245104 (2004).
[6] T. T. Terashima, A. Ikeda, Y. H. Matsuda, A. Kondo, K. Kindo, and F. Iga, J. Phys. Soc. Jpn. **86**, 054710 (2017).

Authors

T. T. Terashima, Y. H. Matsuda, Y. Kohama, A. Ikeda, A. Kondo, K. Kindo, and F. Iga[a]
[a]Ibaraki University

Unconventional Field-Induced Spin Gap in an S = 1/2 Chiral Staggered Chain

P. A. Goddard, T. Sakakibara, and Y. Kohama

The dramatic effect of an alternating local spin environment on the properties of the spin-1/2 antiferromagnetic chain was first discovered through high-field neutron scattering and heat capacity experiments on copper-benzoate, which revealed the development of an energy gap on application of magnetic field [1]. This was perplexing until it was found that the behaviour of this system, and a handful of others, could be described by the sine-Gordon model of quantum-field theory [2,3]. Under the influence of the applied field, the gap emerges thanks to the presence of internal staggered fields and DM interactions that are a direct result of the staggered Cu(II) octahedra.

Here we report on the molecule-based chiral spin chain $[Cu(pym)(H_2O)_4]SiF_6{\cdot}H_2O$ (pym = pyrimidine), which at first glance could be a sine-Gordon chain, but with an added twist: a 4_1 screw (Fig.1(a)). Figure 1(b) shows the frequency evolution of electron-spin resonance at 1.9 K. The observed resonances (black, red and blue (open) squares) cannot be explained by paramagnetic resonances of transition metals or conventional antiferromagnetic resonance. This behavior are reminiscent of excitations observed in the sine-Gordon spin chain $[pym\text{-}Cu(NO_3)_2(H_2O)_2]$, where the branches were identified as breather modes of the sine-Gordon model, along with six other modes more difficult to classify [4]. However, the present observation *cannot* be modeled by the breather gaps proposed for sine-Gordon chains. Figure 1(c) shows the magnetic contribution (C_{mag}) to heat capacity for a deuterated sample of $[Cu(pym)(H_2O)_4]SiF_6{\cdot}H_2O$ down to 100 mK. In zero field above 0.5 K, the nearly constant value of C_{mag}/T can be interpreted as the heat capacity of a uniform S = ½ AF Heisenberg chain in the TLL state. The heat capacity measurement also reveal the field-induced gap in $[Cu(pym)(H_2O)_4]SiF_6{\cdot}H_2O$. Given the similarities with the nonchiral staggered chains, the expression for the temperature dependence of C_{mag} derived from the sine-Gordon model will provide the best possible estimate of the gap at a particular magnetic field. However fitting our data to the sine-Gordon model yields a gap of Δ_s = 1.98 K at 13 T, significantly smaller than the expected value of 8.24 K, calculated using g_{2s} and J values obtained from ESR and magnetometry. More importantly, the field evolution of the gap exhibits $\Delta_s \propto H$, which is distinctly different from the expectation of the sine-Gordon model, where $\Delta_s \propto H^{2/3}$.

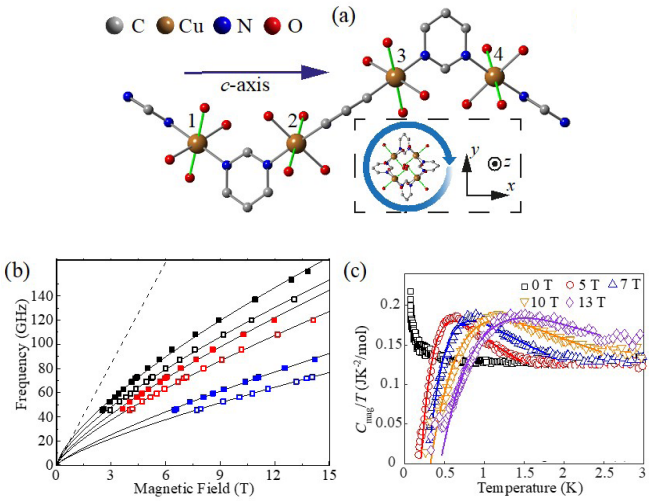

Fig. 1. (a) Chiral structure of $[Cu(pym)(H_2O)_4]SiF_6.H_2O$. (b) Excitations observed via electron-spin resonance at 1.9 K. (c) Temperature dependence of the magnetic contribution to heat capacity at different applied fields showing the opening of a field-induced gap. Lines are fits to a gapped model.

To recap, electron-spin resonance, magnetometry and heat capacity measurements reveal the presence of staggered g tensors, a rich low-temperature excitation spectrum, a staggered susceptibility and a spin gap that opens on the application of magnetic field. These phenomena are reminiscent of those previously observed in non-chiral sine-Gordon systems. In the present case, however, the size of the gap and its measured linear field dependence do not fit with the sine-Gordon model as it stands. We propose that the differences arise due to additional terms in the Hamiltonian resulting from the chiral structure [5].

References

[1] D. C. Dender *et al.*, Phys. Rev. Lett. **79**, 1750 (1997).
[2] M. Oshikawa and I. Affleck, Phys. Rev. Lett. **79**, 2883 (1997).
[3] I. Affleck and M. Oshikawa, Phys. Rev. B **60**, 1038 (1999).
[4] S. A. Zvyagin *et al.*, Phys. Rev. Lett. **93**, 027201 (2004).
[5] J. Liu *et al.*, Phys. Rev. Lett.**122**, 057207 (2019).

Authors

J. Liu[a], S. Kittaka, R. D. Johnson[a], T. Lancaster[b], J. Singleton[c], T. Sakakibara, Y. Kohama, J. van Tol[d], A. Ardavan[a], B. H. Williams[a], S. J. Blundell[a], Z. E. Manson[e], J. L. Manson[e], and P. A. Goddard[f]
[a]University of Oxford
[b]Durham University
[c]National High Magnetic Field Laboratory, Los Alamos National Laboratory
[d]National High Magnetic Field Laboratory, Florida State University
[e]Eastern Washington University
[f]University of Warwick

Oxygen-Functionalization of Graphene Enhances CO_2 Adsorption under Near-Ambient Conditions

S. Yamamoto, J. Yoshinobu, and I. Matsuda

The functionalization of graphene is important in practical applications of graphene, such as in heterogeneous catalysts. The adsorption of molecules on functional-

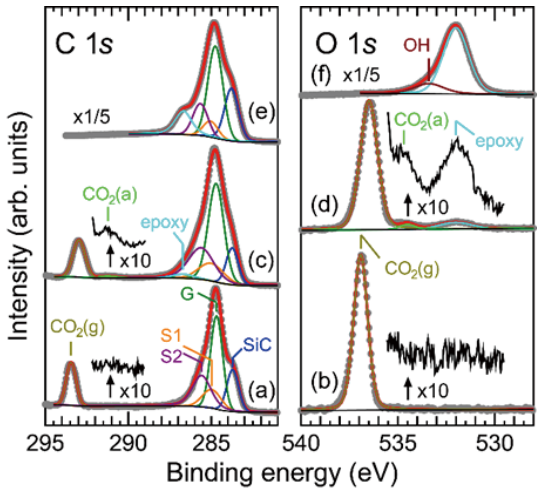

Fig. 1. (a, b) C 1s and O 1s XPS spectra of the pristine epitaxial graphene measured in 1.6 mbar CO_2 at 175 K. (c, d) C 1s and O 1s XPS spectra of the oxygen-functionalized epitaxial graphene measured in 1.6 mbar CO_2 at 175 K. (e, f) C 1s and O 1s XPS spectra of the oxygen-functionalized epitaxial graphene measured in UHV at 199 K after evacuating the CO_2. The incident photon energy was 740 eV. The photon flux densities were 1.0×10^{16} photons/s·cm^2 for (a, b), 7.3×10^{16} photons/s·cm^2 for (c, d), and 1.5×10^{16} photons/s·cm^2 for (e, f). The XPS spectra were normalized with the photon flux densities.

ized graphene is an important elementary step in catalytic reactions on graphene. Despite its importance, however, experimental approaches to clarify the interactions of adsorbed molecules with functionalized graphene are limited. Especially, the experiments in ambient conditions at which catalysts are operated have been challenging.

In this study [1], the adsorption of CO_2 on an oxygen-functionalized epitaxial graphene surface was studied at near-ambient conditions using ambient-pressure X-ray photoelectron spectroscopy (AP-XPS). Monolayer epitaxial graphene on SiC(0001) was used in this study. The oxygen-functionalization of graphene was achieved *in-situ* by the photo-induced dissociation of CO_2 with X-rays on graphene in a CO_2 gas atmosphere. AP-XPS experiments were performed at SPring-8 BL07LSU.

Figures 1(a) and (b) shows C 1s and O 1s XPS spectra of the graphene surface measured under 1.6 mbar CO_2 at 175 K. Except for the spectral features of the substrate (Graphene(G), SiC, and buffer layer (S1 and S2)) and gas-phase CO_2 (CO_2(g)), no adsorbed CO_2 molecules were observed on graphene under the present condition. When the photon flux density was increased by a factor of ~7 under the same conditions of CO_2 gas pressure and sample temperature, C 1s and O 1s XPS spectra were changed (Figs. 1(c, d)). New small peaks at 291.2 eV in C 1s and at 534.7 eV in O 1s XPS spectra were ascribed to adsorbed CO_2 [2]. Figures 1(e) and (f) show the C 1s and O 1s XPS spectra measured in ultrahigh vacuum after evacuating CO_2 gas. After gas evacuation, neither adsorbed CO_2 nor gas-phase CO_2 were observed. Therefore, CO_2 molecules were only present on graphene under near-ambient pressure gas at 175 K. When CO_2 molecules were adsorbed on the graphene surface, additional XPS features were observed at 532.0 eV in O 1s and 286.7 eV in C 1s XPS spectra (Figs. 1(c, d)). These features were assigned to epoxy (C-O-C) group on graphene. The photo-induced dissociation of CO_2 molecules ($CO_2 \rightarrow CO + O$) at high X-ray photon flux causes the formation of epoxy groups on graphene. The oxygen-functionalized graphene surface binds CO_2 molecules more strongly than the pristine graphene surface.

The increase in the adsorption energy of CO_2 on the

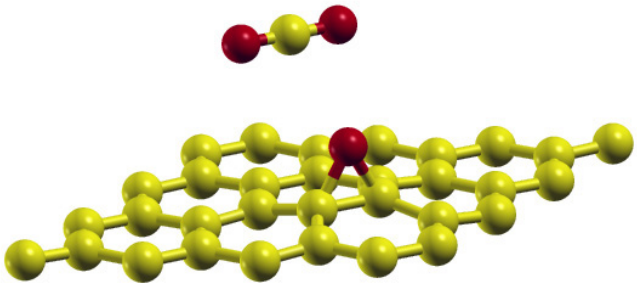

Fig. 2. The structural model of CO_2 adsorbed on the oxygen-functionalized graphene. The oxygen species on graphene is an epoxy (C-O-C) group.

oxygen-functionalized graphene surface was further investigated by first-principles calculations with the van der Waals density functional (vdW-DF) method. The adsorption energy of CO_2 was increased by ~5 kJ/mol from 20.2 kJ/mol on the pristine graphene surface [2] to 25.7 kJ/mol on the oxygen-functionalized graphene surface. This was in good agreement with the experimental value (≥ 5 kJ/mol) derived from an adsorption and desorption equilibrium relationship. In addition, first-principles calculations revealed that the most stable adsorption site of CO_2 on the oxygen-functionalized graphene surface was not on top of the epoxy group, but on the C-C bond of graphene adjacent to the epoxy group (Fig. 2). The adsorption of CO_2 on the oxygen-functionalized graphene surface was stabilized by both the electrostatic interactions between the CO_2 and epoxy group and the vdW interactions between the CO_2 and graphene. The detailed understanding of the interaction between CO_2 and the oxygen-functionalized graphene surface obtained in the present study may assist in developing guidelines for designing novel graphene-based catalysts.

References

[1] S. Yamamoto, K. Takeuchi, Y. Hamamoto, R.-Y. Liu, Y. Shiozawa, T. Koitaya, T. Someya, K. Tashima, H. Fukidome, K. Mukai, S. Yoshimoto, M. Suemitsu, Y. Morikawa, J. Yoshinobu, and I. Matsuda, Phys. Chem. Chem. Phys. **20**, 19532 (2018).

[2] K. Takeuchi, S. Yamamoto, Y. Hamamoto, Y. Shiozawa, K. Tashima, H. Fukidome, T. Koitaya, K. Mukai, S. Yoshimoto, M. Suemitsu, Y. Morikawa, J. Yoshinobu, and I. Matsuda, J. Phys. Chem. C **121**, 2807 (2017).

Authors

S. Yamamoto, K. Takeuchi, Y. Hamamoto[a], R.-Y. Liu, Y. Shiozawa, T. Koitaya, T. Someya, K. Tashima[b], H. Fukidome[b], K. Mukai, S. Yoshimoto, M. Suemitsu[b], Y. Morikawa[a], J. Yoshinobu, and I. Matsuda

[a]Osaka University

[b]Tohoku University

Ultrafast Control of a Ferroelectricity with Dynamic Repositioning of Proton in a Supermolecular Cocrystal

T. Umanodan, Y. Okimoto, and J. Itatani

Recent progress of intense THz and mid-IR (MIR) sources has opened a new opportunity in solid state physics. The small photon energy that is associated to long wavelength enables to nondestructively apply intense optical fields (~10 MV/cm or higher) to condensed matters because multiphoton ionization followed by catastrophic optical damage is unlikely to occur. When materials, especially crystalline materials, are exposed to such intense

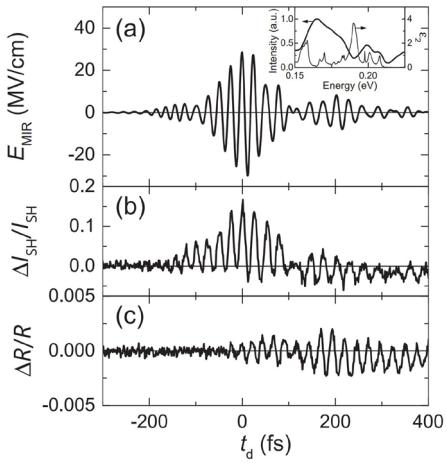

Fig. 1. (a) Waveform of the MIR pulse used for photoexcitation. The inset depicts the power spectrum of the pulse. The thin line shows the ε_2 spectrum of Hdppz-Hca. (b) and (c) Time profile of $\Delta I_{SH}/I_{SH}$ (b) and relative change in the reflectivity ($\Delta R/R$) (c) in the presence of a MIR field.

optical fields, many nontrivial exotic phenomena (e.g., high harmonic generation in solids) start to occur.

In this work, we explored the possibility of ultrafast control of ferroelectricity in a supraziramolecular ferroelectric cocrystal composed of protonated 2,3-di(2-pyridinyl) pyrazine (Hdppz) and deprotonated chloranilic acid (Hca). The crystal becomes ferroelectric due to proton ordering below the Curie point (Tc = 402 K), where the protons take two stable positions between the Hdppz and Hca molecules. We used intense THz and MIR pulses with stable carrier envelope phases, and probed the symmetry breaking in the presence of optical field using 6.5-fs optical pulses. This pulse duration is shorter than one oscillation period of the driving low frequency field, which allows to look into field-induced proton dynamics on sub-cycle time scales of the MIR field. We measured second harmonic of ultrashort visible pulses as a signature of inversion symmetry breaking due to proton displacement.

Figure 1(a) and (b) show the electric field waveform of the intense MIR pulses and observed change of second harmonic (SH) signals, respectively. Although the MIR field contains multiple cycles (i.e., the envelopes of the positive and negative polarity are identical), observed SH signal follows the optical waveform of the positive polarity alone. This behavior is well reproduced by a classical model depicted in Fig. 2. In this model, we included anharmonic potential and molecular vibration whose resonant frequency is within the MIR spectrum. As shown in the inset in Fig. (a)), the spectrum of driving MIR pulse has an overlap with an absorption peak of C-O$^-$ stretching mode, leading to the displacement of equilibrium point in the presence of MIR fields. Contrary, with an intense THz field, the change of SH signals was observed to be proportional to the instantaneous field amplitude.

In summary, using intense THz and MIR pulses, we observed field-induced symmetry breaking in Hdppz-Hca molecular crystals. This process can be understood as the proton displacement that can follow the oscillating optical field up to ~100 THz. The results suggest that repositioning of protons and resulting ferroelectricity can be dynamically controlled by the optical waveform of intense optical pulses. We expect that more exotic nonlinear responses will be discovered in future, leading to a foundation of PHz optoelectronics.

Reference

[1] T. Umanodan, K. Kaneshima, K. Takeuchi, N. Ishii, J. Itatani, H. Hirori, Y. Sanari, K. Tanaka, Y. Kanemitsu, T. Ishikawa, S. Koshihara, S. Horiuchi, and Y. Okimoto, J. Phys. Soc. Jpn. 88, 013705 (2019). [Selected as an Editors' Choice]

Authors

T. Umanodan[a], K. Kaneshima, K. Takeuchi, N. Ishii, J. Itatani, H. Hirori[b], Y. Sanari[b], K. Tanaka[b], Y. Kanemitsu[b], T. Ishikawa[a], S. Koshihara[a], S. Horiuchi[c], and Y. Okimoto[a]

[a]Tokyo Institute of Technology

[b]Kyoto University

[c]National Institute of Advanced Industrial Science and Technology (AIST)

Tensile-Strain-Dependent Spin States in Epitaxial $LaCoO_3$ Thin Films

Y. Yokoyama, H. Wadati, and Y. Harada

In transition metal compounds, charge, spin, and orbital degrees of freedom by a strong electron correlation realize various physical phenomena such as superconductivity, metal-insulator transition, and charge ordering [1]. The perovskite-type cobalt oxide $LaCoO_3$ is one of the most interesting materials because of its various electron degrees of freedom. Since the spin state of $LaCoO_3$ is sensitive to the crystal field, a spin crossover from the low-spin (LS) to high-spin (HS) state is shown by increasing the temperature [2]. Epitaxial strain can also influence the spin states and a ferromagnetism is observed in $LaCoO_3$ thin films at lower temperatures ($\lesssim 85$ K) [3–5]. In previous studies, the spin states of the thin films were considered by the orderings of 3d electrons on the basis of resonant x-ray diffraction [3–5]. However, direct observations of the electronic structures are important to clarify the spin states. Since it is difficult to determine the spin states by conventional techniques such as x-ray absorption spectroscopy (XAS), we performed resonant inelastic soft x-ray scattering (RIXS) with Co 2p $\rightarrow$ 3d $\rightarrow$ 2p process (L edge) [6]. The RIXS is one of the most powerful techniques to clarify the spin states by observing the d-d excitations.

The $LaCoO_3$ epitaxial thin films (30 nm thickness) were fabricated on LSAT(110) and LSAT(111) [$(LaAlO_3)_{0.3}(SrAl_{0.5}Ta_{0.5}O_3)_{0.7}$] substrates by pulsed laser deposition

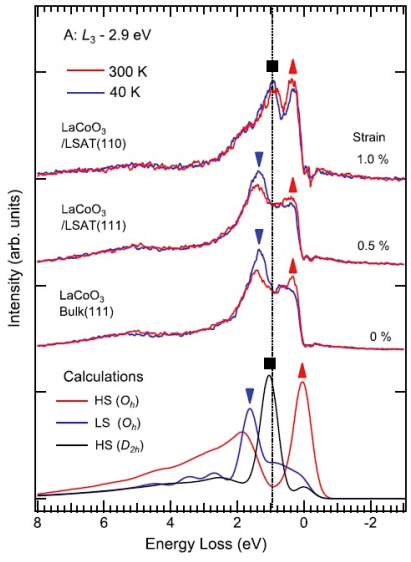

Fig. 1. Comparison of the experimental RIXS spectra excited with A: L_3 –2.9 eV (776.5 eV) measured at 40 and 300 K and the theoretical ones in O_h and D_{2h} symmetries.

technique. The same substrates with different orientations enable us to observe the pure strain effects on XAS and RIXS spectra. The lattice constant of the LSAT substrate is 3.868 Å, while that of the $LaCoO_3$ bulk is 3.804 Å, indicating that tensile strains are applied to the $LaCoO_3$ epitaxial thin films grown on LSAT substrates. The magnitude of the tensile strains from LSAT(110) and LSAT(111) substrates are 1.0% and 0.5%, respectively (strains are defined as the ratio of the cubic root of the unit cell volume) [3,4]. The experiments of XAS and RIXS were performed at BL07LSU HORNET, SPring-8 [7]. The RIXS measurements were performed with soft x-ray from 770 to 810 eV (Co L_3 and L_2 edge). In the range of the x-ray energy, the energy resolution is ~ 300 meV.

The comparison of the experimental RIXS spectra excited with A: L_3 −2.9 eV (776.5 eV) measured at 40 and 300 K and the theoretical ones with several electronic states are shown in Fig. 3. The peaks observed at around 0.3 eV is assigned to the excitations from the HS ground states. On the other hand, the peaks at 1.3 eV observed correspond to the excitations from the LS ground states. However, the peaks at 1.0 eV in $LaCoO_3$/LSAT(110) cannot be explained by either the LS or HS with O_h symmetry. By comparing with the theoretical spectra, the peak for the HS state is shifted to 1.0 eV by lowering the symmetry from O_h to D_{2h}, indicating that the spin state of $LaCoO_3$/LSAT(110) consists of the HS states with different local symmetries, i.e., the mixture of O_h and D_{2h} symmetries.

In this study, we performed RIXS measurements and revealed that the spin states of Co ions were different between the bulk crystal and the thin film crystals. Although it is difficult to observe the strain effects on the spin states with conventional XAS measurements, clear difference can be probed with the use of RIXS.

References

[1] M. Imada *et al*., Rev. Mod. Phys. **70**, 277 1039 (1998).
[2] M.W. Haverkort *et al*., Phys. Rev. Lett. **97**, 176405 (2006).
[3] J. Fujioka *et al*., Phys. Rev. Lett. **111**, 027206 (2013).
[4] J. Fujioka *et al*., Phys. Rev. B **92**, 195115 (2015).
[5] Y. Yamasaki *et al*., J. Phys. Soc. Jpn. **85**, 023704 (2016).
[6] Y. Yokoyama *et al*., Phys. Rev. Lett. **120**, 206402 (2018).
[7] Y. Harada *et al*., Rev. Sci. Instrum. **83**, 013116 (2012).

Authors

Y. Yokoyama, Y. Yamasaki, M. Taguchi, Y. Hirata, K. Takubo, J. Miyawaki, Y. Harada, D. Asakura, J. Fujioka, M. Nakamura, H. Daimon, M. Kawasaki, Y. Tokura, and H. Wadati

Photo-Induced Semimetallic States Realized in Electron–Hole Coupled Insulators

K. Okazaki, T. Mizokawa, and S. Shin

Using light to manipulate materials into desired states is one of the goals in condensed matter physics, since light control can provide ultrafast and environmentally friendly photonics devices. However, it is generally difficult to realize a photo-induced phase which is not merely a higher entropy phase corresponding to a high-temperature phase at equilibrium.

Here, we report realization of photo-induced insulator-to-metal transitions in $Ta_2Ni(Se_{1-x}S_x)_5$ including the excitonic insulator phase using time- and angle-resolved photoemission spectroscopy (TARPES) [1]. From the dynamic properties of the system, we determine that screening of excitonic correlations plays a key role in the timescale of the transition to the metallic phase, which supports the existence of an excitonic insulator phase at equilibrium. The nonequilibrium metallic state observed unexpectedly in the direct-gap excitonic insulator opens up a new avenue to optical band engineering in electron–hole coupled systems.

Figure 1 shows the time-integrated TARPES spectra before and after pumping. After photo-excitation, both the electron and hole bands cross E_F at the same Fermi momentum k_F ~0.1 A^{-1} as schematically shown by the red and blue parabolas in Fig. 1b. This may indicate that the hybridization between the two Ta chains is sufficiently strong to lift the degeneracy. However, since this is not predicted by band-structure calculations, this behavior of the emerging of the hole and electron bands crossing E_F at the same k_F is a surprising nature of the observed non-equilibrium metallic phase, indicating that the observed nonequilibrium metallic state is entirely different from the high temperature phase in the equilibrium state.

To confirm that the observed non-equilibrium metallic phase of Ta_2NiSe_5 can be associated with the excitonic condensation, we have performed comparative TARPES measurements on Ta_2NiS_5. Quite unexpectedly, an electron band emerges above E_F and the hole band below E_F shifts upward. In addition, the bottom of the electron band and the top of the hole band seems to cross E_F, and the system seems likely to be semimetallic. This may require reconsidering the nature of the insulating phase for Ta_2NiS_5, which had been considered as an ordinary band insulator.

The non-equilibrium metallic phases observed for both of Ta_2NiSe_5 and Ta_2NiS_5 should suggest that these photo-induced phase transitions are not merely transitions to higher entropy states that can be realized at high temperatures in the equilibrium state. Thus, photo-excitation can be considered to induce similar effects to pressure. Since the pressure-induced superconducting phase has been found for Ta_2NiSe_5, with some appropriate pumping condition probably with lower photon energy of some resonant condition, photo-induced superconductivity might be realized for

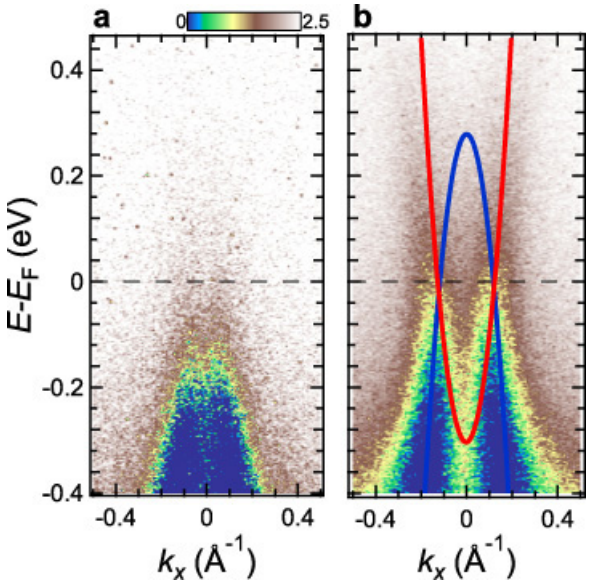

Fig. 1. TARPES spectra of Ta_2NiSe_5 before and after pumping. **a** Energy–momentum (E–k) map before pumping, integrated in the time interval [–0.29, 0] ps. **b** Corresponding map of the transient states, integrated in [0, 1.2] ps. Red and blue parabolas indicate the electron and hole bands crossing E_F in the non-equilibrium metallic state. These spectra were acquired with a pump fluence of 1.56 mJ/cm^2.

this material. Realization of this fascinating photo-induced phase would be one of the ultimate goals of investigations of the photo-excited electronic state.

Reference
[1] K. Okazaki, Y. Ogawa, T. Suzuki, T. Yamamoto, T. Someya, S. Michimae, M. Watanabe, Y.-F. Lu, M. Nohara, H. Takagi, N. Katayama, H. Sawa, M. Fujisawa, T. Kanai, N. Ishii, J. Itatani, T. Mizokawa, and S. Shin, Nat. Commun. **9**, 4322, (2018).

Authors
K. Okazaki, Y. Ogawa, T. Suzuki, T. Yamamoto, T. Someya, S. Michimae, M. Watanabe, Y.-F. Lu[a], M. Nohara[b], H. Takagi[a,c], N. Katayama[d], H. Sawa[d], M. Fujisawa, T. Kanai, N. Ishii, J. Itatani, T. Mizokawa[e], and S. Shin
[a]University of Tokyo
[b]Okayama University
[c]Max Planck Institute for Solid State Research
[d]Nagoya University
[e]Waseda University